Acta Materialia xxx (xxxx) xxx

Contents lists available at ScienceDirect

Acta Materialia

journal homepage: www.elsevier.com/locate/actamat

Overview article

On the preparation and mechanical testing of nano to micron-scale specimens

Luciano Borasi [a], Alejandra Slagter [a], Andreas Mortensen [b], Christoph Kirchlechner [c,*]

[a] Department of Materials Science and Engineering, McCormick School of Engineering and Applied Science, Northwestern University, Evanston, IL 60208, USA
[b] Laboratory of Mechanical Metallurgy, École Polytechnique Fédérale de Lausanne, Lausanne, CH-1015, Switzerland
[c] Institute for Applied Materials (IAM), Karlsruhe Institute of Technology, Kaiserstrasse 12, D-76131 Karlsruhe, Germany

ARTICLE INFO

Keywords:
Ion beam processing
Ion irradiation
Micron scale
Mechanical properties
Size effect

ABSTRACT

Over the past two decades, means allowing to probe experimentally the mechanical behavior of materials specimens only a few micrometers or less in diameter have multiplied, largely owing to the widespread adoption and versatility of focused ion beam (FIB) milling for the preparation of small-scale test specimens. Despite its remarkable capabilities, the ion bombardment that is employed during FIB milling operations does not leave machined surfaces unscathed: it may induce a series of alterations in the near-surface microstructure of materials, which vary in severity depending on the material being milled, or milling parameters, or the type of ion used. These alterations in turn can strongly influence the local behavior, and as a result measured mechanical properties, of the milled material. In the first part of this manuscript, we review the different forms that FIB-induced microstructural alterations can take and their influence on small-scale mechanical test results. In the second part, we present alternative strategies that have been used to circumvent the issue. These include the use of entirely different small-scale sample fabrication processes, as well as approaches that do use FIB-milling but put effort in the test design to minimize or avoid the formation of FIB-induced defects in regions where micromechanical test data are collected. The advent of such methods can enhance our understanding of FIB-induced defects on the mechanical behavior of microsamples by comparing the results with those from ion-milled samples. This, in turn, should improve our ability to interpret test data when FIB-milling is the only method available for microsample production.

1. Introduction

Twenty years have passed since Uchic, Dimiduk, Florando and Nix disclosed to the scientific community an ingenious method for the preparation of small, micron-scale, compression test samples, often called “nanopillars”, by means of which one can measure the plastic deformation law of samples so small that their size affects their response [1,2]. The method is so rich and comparatively easy to implement that it has generated a wave of follow-on studies that have used it, nearly unchanged, to measure the plastic deformation law of small-scale samples cut into a wide range of materials. This test is still extensively used and has now been extended to probe the influence of high strain rates, strain rate variations, cyclic loading or elevated temperature. It has also been extended to produce a wide range of other sample geometries, including tensile or notched bend bars, enabling for example the measurement of fracture toughness. Several reviews describe this extensive body of work, exposing and discussing the many questions that micromechanical test data have raised, such as the raised flow stress and the jagged shape of resulting stress-strain curves, or challenges that appear in measuring an unambiguous fracture toughness when sample sizes fall below a few micrometers [3–22]. Focused ion beam (FIB) milling is most often used to prepare micromechanical test samples owing to its ability to accurately carve variously shaped micro- to nanoscale specimens into polished metallographic surfaces of the material to be characterized (Fig. 1). Widespread adoption of the method has further gained momentum with the pursuit of scientific questions raised by the data it produces, such as the plasticity size-effect, measured in samples deformed essentially in the absence of strain gradients [2,23].

Despite its remarkable capabilities, the ion bombardment that is used in FIB milling to remove material does not leave the microstructure of machined surfaces unscathed: vacancies and interstitials, implanted beam atoms and punched dislocations are typical artifacts that line the

* Corresponding author.
E-mail address: christoph.kirchlechner@kit.edu (C. Kirchlechner).

https://doi.org/10.1016/j.actamat.2024.120394
Received 25 April 2024; Received in revised form 8 September 2024; Accepted 10 September 2024
Available online 14 September 2024

surface of ion-milled samples, to a depth that depends strongly on the ionic species making the beam together with the beam energy. This issue has long been identified; however, we find that it has received insufficient attention, as the impact of these defects on small-scale test mechanical property data has on several occasions been found to be significant. While qualitative analysis and relative comparisons of properties across samples that were prepared identically of course retain their validity, awareness of the unique microstructural signatures imparted on the material by the processing method that was used to prepare samples is a strong imperative in reporting and interpreting the mechanical behavior of materials at the microscale.

We examine, in this review of the literature, the influence of FIB-induced defects on small-scale mechanical testing outcomes, to stress the need for attention to the matter and to also show that there are strategies that enable micromechanical testing of materials free of the surface microstructure alterations that often come with FIB-milling. We first summarize, based on literature data, the nature (Section 2), and the potential consequences of FIB-induced surface damage on micromechanical test data (Section 3). Given that these experiments predominantly use in-situ SEM/TEM techniques, Section 3 also discusses the effect of electron bombardment on test outcomes for certain materials. In the second half of this review, we present alternative strategies that have been used to circumvent the issue (Section 4). This includes an overview of available techniques that altogether exclude FIB-milling in the production and/or characterization of small-scale structures, followed by coverage of strategies that use FIB-milling but design the test to minimize or avoid entirely the presence of FIB-induced defects in regions where micromechanical test data are collected. We then conclude with a motion for greater openness and rigor in reporting micromechanical test data.

2. Nature of focused ion beam milled material modification

Milling operations using a FIB are possible because accelerated ions cause, upon hitting the surface of a sample of solid material, its forced removal. This, coupled with the focused nature of the ion beam, enables localized milling and the fabrication of shaped components with submicron resolution that have a geometry only restricted by the accessibility of the beam to the material through its initial surface [27–31]. Typically used ions are of gallium, although nowadays other options such as xenon, neon [32], and helium are available [33].

The primary limitation of FIB milling is intricately linked to the fact that, in addition to the sputtering of material, other modes of interaction come into play during ion bombardment of material surfaces; Ref. [34] provides a comprehensive review of the interaction between ions and solid surfaces. Ion-milling can induce chemical and physical damage in regions in close proximity to the milled surface, leading to drawbacks in the technique that can be minimized, but not eliminated, by performing the last steps of the milling process at low energy (see following sections).

Another issue with the technique is that top-down milling, when used to carve nanopillars, generally leads to pillar tapering, which in turn induces a non-uniform stress state along the pillar during testing. Friction against the punch at the top surface coupled with the sample being attached at its base to the material into which it was carved, also create complex triaxial stress states within the nominally uniaxial compression sample, either at sample ends, or along its length if it barrels [35–37]. These deviations in stress state away from the uniaxial stress that is generally assumed to be obtained along the pillar can cause, in turn, significant discrepancies between the true response of the material and what is found in load-displacement data. To prevent tapering, supplementary lateral milling operations are often conducted as a finishing milling step, a fabrication process frequently termed lathe milling [23]. Complex shapes, namely dog-bone specimens, or the machining of larger (10 μm or more) diameter pillars, also require longer milling times, resulting in high sample production costs. These issues are to some extent being alleviated now that Xe plasma FIB systems outpace the conventional Ga FIB in terms of milling speed by a significant margin [38]. Also, the recent emergence of laser-focused ion beam (LaserFIB), and femtosecond laser-assisted FIB-milling represents a significant advancement in this regard [39–41], as milling rates achievable with femtosecond laser technology far surpass those of conventional FIB sources currently employed, demonstrating orders of magnitude improvement. The use of these technologies, however, remains to date quite limited.

Time limitations and limits associated with the range of geometries that can be achieved by ion beam milling are, however, secondary in comparison with the principal drawback associated with FIB-milled micromechanical test samples, namely that milled surfaces are lined with a layer of material that differs from that which is nominally to be tested. Furthermore, on occasions, material removed during FIB milling can recombine and lead to the formation of redeposited layers that land upon sections of the sample that intervene in the micromechanical test, thus again affecting the data produced.

2.1. Chemical artifacts

Chemical artifacts can be expected if the ion species used for milling presents affinity for elements in the material being milled. While inert gas ions – specifically He, Ne, Ar and Xe – are typically not expected to chemically interact with the material of interest (although the formation of a helide compound after He irradiation has been recently reported [42]), all other ion species, including Ga, might do so and therefore can produce a substantial modification of the material and its properties. Examples of this are the formation of Cu_3Ga when milling copper with a focused Ga ion beam, Fig. 2A [43,44], hydride formation in Zr alloys (where, even when residual hydrogen in the initial chemical composition is negligible, specific conditions reached during FIB milling are believed to trigger dissociation of hydrogen-containing impurities in the vacuum chamber, enabling hydrogen to diffuse into the specimen) [45,

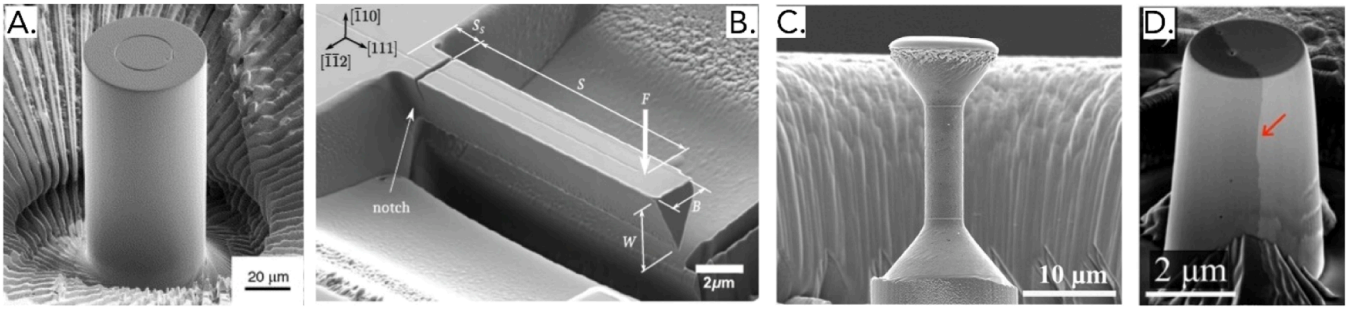

Fig. 1. Various FIB-milled structures that have been produced for micromechanical testing. (A) Micropillar machined into a Ni_3(Al, Hf) single-crystal. Reprinted from [23] with permission from Elsevier. (B) Microcantilever beam machined into monocrystalline silicon [24]. (C) Dog-bone tensile specimen machined into the surface of a high entropy alloy [25]. (D) A copper micropillar containing an incoherent boundary (red arrow) [26].

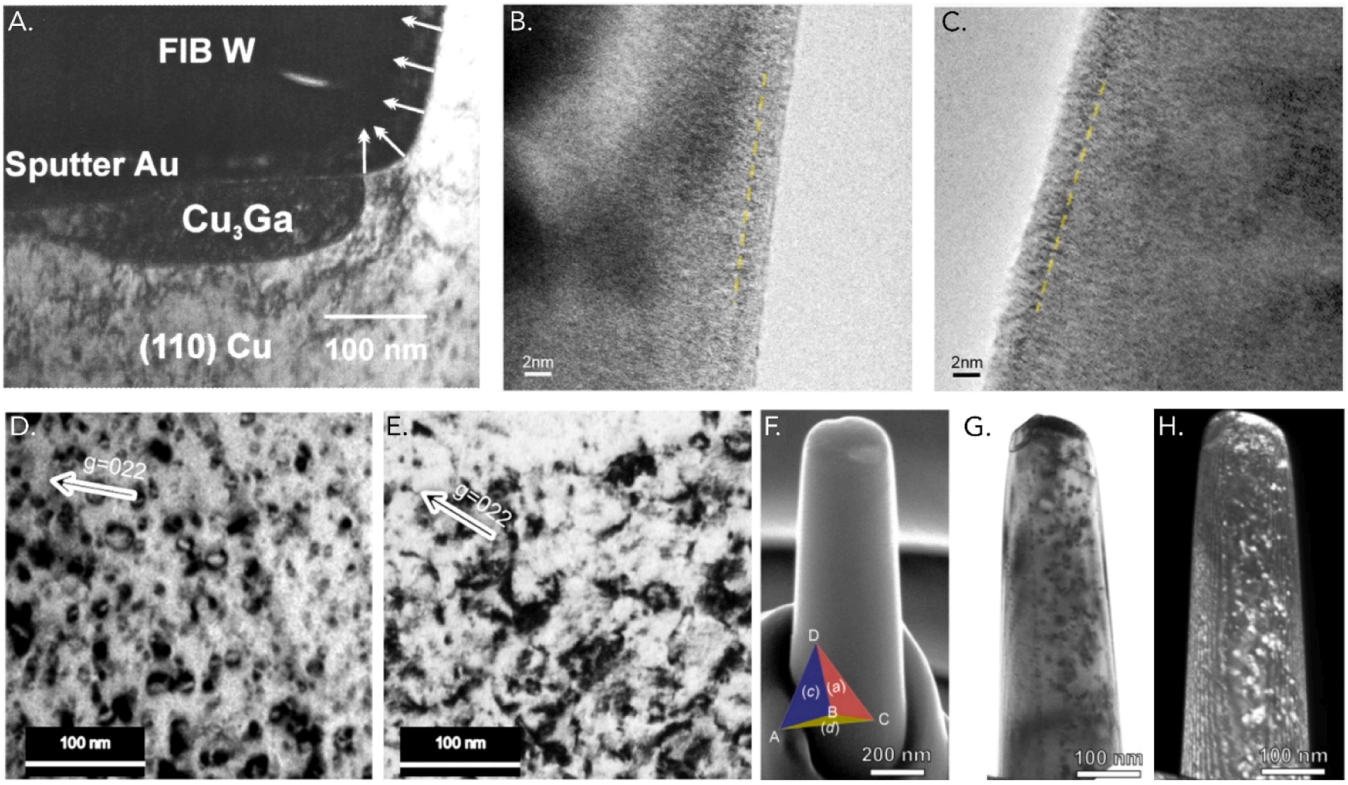

Fig. 2. Defects produced by the FIB. (A) A copper FIB-milled lamella, protected by sputtered gold and FIB-deposited W, showing a Cu_3Ga phase formed during milling operations. Reprinted with permission from [43] Copyright 2002, American Vacuum Society. (B-C) Bright field (BF) TEM images displaying amorphization in aluminum caused by xenon and gallium FIB-milling, respectively [54]. (D-E) BF TEM images showing FIB-induced dislocation loops in aluminum using Ga and Xe ions, respectively [54]. (F) SEM and (G-H) TEM images exhibiting the presence of dislocation loops on FIB-milled sub-micron aluminum pillars. (F-G-H) Reprinted from [66] with permission from Elsevier.

46] or the well-known [47–49] observation that gallium segregates to, and embrittles, aluminum grain boundaries [50–52].

The severity of resulting material alterations varies with both the milled material and type of ion used [53]. Significant chemical interactions between the material and the incoming, highly energetic, ionized species pose a fundamental challenge, potentially rendering characterization techniques using FIB-milled samples impractical if the composition of the material to be tested deviates significantly from its original state or intended composition.

2.2. *Physical artifacts*

Besides chemical artifacts caused by chemical affinity between the material and the ion species, interaction of the focused ion beam with the material surface induces several possible substructural alterations that are physical in character and linked to the high impact energy of the incoming ions [55].

The energetic ion interactions in the near surface region do not only sputter near-surface atoms and result in the wanted material removal, but also cause displacements of atoms that are not sputtered away, a phenomenon that arises in a sub-surface volume where the energy delivered by the incoming ions is sufficient to break atomic bonds in the material. In the worst case, the displacement results in an amorphization of the material [56–60]. Several transmission electron microscopy (TEM) analyses have evidenced the presence of such an amorphous layer (Fig. 2B-C) in diverse materials [54,57,58,60], while in some systems a modified layer of material was found to be produced by an ion-induced phase transformation [60–62]. Moreover, ion and even electron beam irradiation have been reported to induce various degradation mechanisms such as cross-linking or chain scission in polymers [63–65].

Even in the absence of amorphization, the displacement of lattice atoms is not fully reversible, and a high density of point defects can be expected in the FIB-milled area. The formation of vacancies and interstitials is referred to as "*knock-on damage*". To the best of the authors' knowledge, there are no systematic experimental studies of vacancy densities in FIB-milled samples; however, ample evidence of microstructural modifications caused by the high energy ion impact can be found when these point defects coalesce to form dislocation loops [66–68] (Fig. 2D-H) or in some cases even nano-pores [69,70]. FIB-milled micropillars of Si, Al and Au were shown as far back as 2006 to contain altered dislocation structures and elastic strain gradients [71–73]. The effect of knock-on damage is furthermore not restricted to gallium ion beams; for instance, helium irradiation has been reported to cause the formation of sub-micron bubbles [42,74–76]. Monte Carlo simulations integrated into the *Stopping and Range of Ions in Matter* (SRIM) package can be employed to compute the atomic displacements per atom (dpa); Ref. [77] provides a comprehensive overview on the use of SRIM, while Refs. [42,53,60,78] present good examples of the potential of SRIM to predict damage for different materials and milling conditions.

The high beam energy can cause implantation of the ionic species within the material. Ion implantation, even in the absence of chemical segregation and in the most basic scenario, leads to the formation of a substitutional solid solution between the ion species and the material. This process occurs across the spectrum of incoming ion energies, with higher energies resulting in deeper implantations. This modification of the material along the specimen surface is likely to impact properties such as the yield strength, stacking fault energy, or fracture toughness. Another consequence of ion implantation are residual stresses coupled with changes in the lattice parameter, which can strongly influence the local mechanical behavior of milled material (see e.g., data for alumina [79] and the discussion in Section 3). Unfortunately, SRIM calculations

have been shown to significantly underestimate the depth to which ions penetrate in crystalline materials, a limitation ascribed to the fact that SRIM neglects the crystalline structure of the material and the channeling of ions along crystallographic planes or directions, which can lead to deeper implantation [53].

Similar to chemical interactions, the extent and nature of the FIB-induced physical artifacts strongly depends on the material of interest. In addition, milling conditions such as the incident angle [23,80,81] and ion energy [57,82] are known to exert an important influence on the final shape and artifacts generated. For example, Ref. [81] reports that, in silicon, normal milling resulted in both a higher gallium concentration and a wider spreading distance compared to milling under glancing incidence. Moreover, when subjected to a 30 kV Ga beam, silicon exhibited an amorphous layer of thickness ranging from 20 to 30 nm [57,83] while a 4 nm thick layer was observed in a 7075 aluminum alloy [82] and copper specimens showed no evidence of an amorphous layer under conditions that readily amorphized silicon [84]. Auger electron spectroscopy (AES) has unveiled surface-rich gallium concentration profiles that vary as a function of the milling current (and ion dose) [67]. Fig. 3a illustrates an increase in the maximum Ga concentration as the ion dose is varied by changing the ion current for a fixed exposure time of 30 s on the sample surface, reaching values as high as 12 at% at a depth of 10 nm. Additionally, Fig. 3b shows the effect of microstructure on the concentration versus penetration depth of gallium by comparing an ultra-fine grained (UFG) copper produced by severe plastic deformation with monocrystalline copper. The UFG copper exhibited a smaller penetration depth but a higher peak Ga concentration. The reduced penetration depth was ascribed to the diverse crystal orientations within UFG copper, which inhibit channeling. The higher density of structural defects in the UFG copper was reported to be the reason underlying the higher maximum Ga concentration in the near surface compared to the single-crystal. Similar analyses of the implantation of Xe, Ar, N and O in tungsten atom probe specimens were investigated as a function of the acceleration voltage in [53], with Xe exhibiting the lowest implantation depth.

2.3. The role of redeposited material

During FIB milling, removed material can recombine, forming redeposited layers. This redeposited material has a different structure, and often also another chemical composition, than the material to be tested. It can be expected that redeposited material predominantly consists of the material of interest and Ga, but traces of residual gas present in the FIB chamber also contribute to the overall composition. An example of the distribution of Ga in the redeposition layer (in this case far from the region of interest) is shown in Fig. 4. Redeposition typically shows island growth first. In the case of pronounced island growth, redeposited material can be made visible in most dual beam FIB

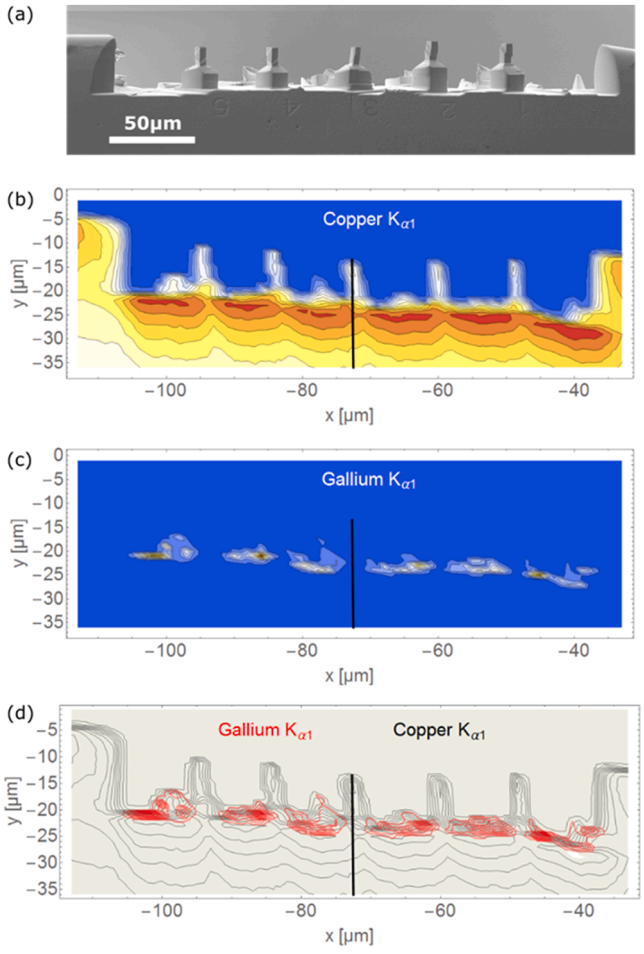

Fig. 4. Scan of five copper micropillars located along an electrolytically polished edge of a copper bi-crystal containing a grain boundary (black vertical line). The redeposition layer consists of Cu and Ga. (a) SEM micrograph of the sample, (b) Cu-$K_{\alpha1}$, (c) Ga-$K_{\alpha1}$, and (d) an overlay of Cu-$K_{\alpha1}$ and Ga-$K_{\alpha1}$. Reproduced from [85] with permission from its author.

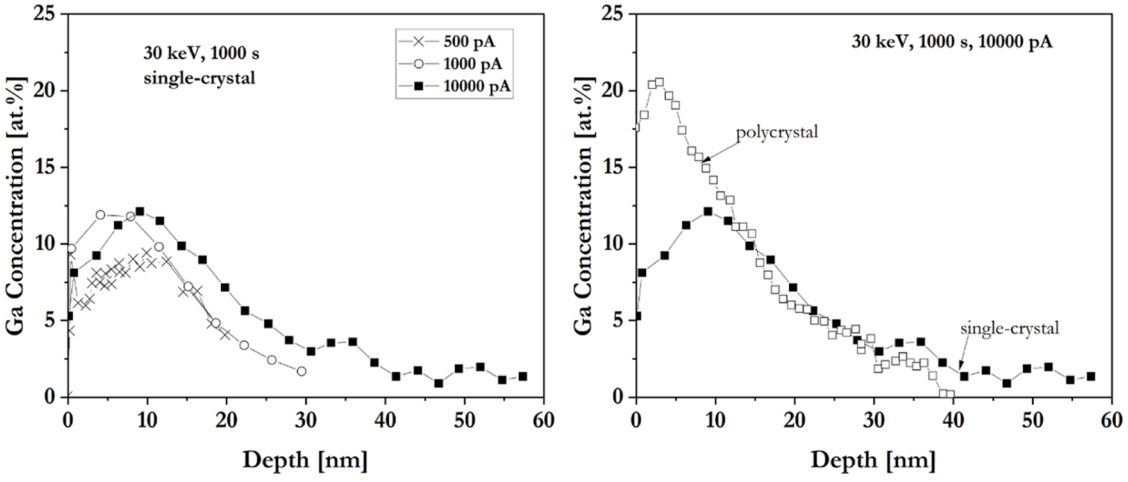

Fig. 3. Auger electron spectroscopy (AES) depth profiles of gallium in monocrystalline copper and in a 300 nm grain size polycrystalline and plastically deformed copper specimen. The impact of the milling current is also displayed. Reprinted from [67] with permission from Elsevier (redrawn for image quality purposes only).

systems by low voltage electron imaging during FIB milling. Examples are shown in Fig. 5A over a limited region (marked with an arrow) and in Fig. 6A. As soon as continuous film growth dominates, however, redeposition layers become less visible, and their identification becomes difficult, if not impossible. Fig. 5 illustrates a particle exposed through preferential chemical etching of the base material (steps 1 and 2 in the inset of Fig. 5A). Subsequently, a notch was created in this particle using FIB milling, resulting in a redeposition layer (step 3 in the inset of Fig. 5A). Although this redeposition layer is barely discernible in the SEM analysis (indicated by the arrow in Fig. 5A), it becomes evident after further chemical etching of the base material, which leaves behind the non-etched redeposited layer (Fig. 5B). Smooth redeposition layers can only be made visible by preparing a cross-section, e.g. when milling a rectangular micro pillar and tuning imaging parameters so as to maximize the contrast between the material and the redeposition layer (see Fig. 6B-C), as otherwise this layer will generally not be visible in SEM, as can be seen in Fig. 5A in regions other than that indicated with an arrow. In circular micropillars, where the entire sample surface can be homogeneously covered with redeposition, to the best knowledge of the authors, there is no established way to detect this layer before sample testing, as it does not exhibit pronounced contrast during SEM imaging or alterations in surface topography.

Due to these alterations in chemical composition and microstructure, entirely different elastic, plastic, and fracture properties compared to the material can be expected for redeposition layers, and therefore for data collected over a sample that comprises stressed redeposited material. Until today there are – to the best of the authors' knowledge – no systematic studies on the effect of redeposition layers on the mechanical response of small-scale specimens; however, already some consequences are qualitatively known and include the following.

A continuous redeposition layer blocks – similar to a native oxide layer – the escape of dislocations through the sample surface [86]. This may cause the formation of dislocation pile-ups and therefore might hamper or skew the analysis of post mortem dislocation structures. Slip steps otherwise found along surfaces of crystalline micro pillars are then not formed and therefore active slip systems cannot be identified by post-test micro pillar topographies [80]. While the impact of this effect on mechanical properties – see next section – also strongly depends on the sample size, the absence of clear slip steps and the pile-up of dislocations can result in misinterpretations of micro pillar compression experiments [87].

A further known consequence of redeposition layers is their grown-in residual stress. Due to the comparable dimensions of redeposition layers on one hand, and remaining materials in micron and submicron sized specimen on the other hand, stress levels of similar magnitude as in the redeposition layer are imposed on the nearby material. Since the redeposition layer is furthermore typically not homogenous – i.e., its thickness varies – residual bending moments can also be transmitted to the material, resulting in deviatoric strain gradients, i.e., lattice curvature. This, in turn, can lead to possible misinterpretations of diffraction data, as concerns for example the estimation of GND densities [88] (or could also perhaps explain unexpected peak streaking features that were observed in Laue experiment data collected on nanopillars in Ref. [71]).

In contrast to the chemically and physically induced damage of FIB-milled surfaces (Sections 2.1 & 2.2), the effect of redeposition layers can mostly or even entirely be avoided by good scientific practice. Besides the milling rate (ideally low to keep the local partial pressure of ions small, enabling them to be removed into the pumping system and minimize additional collisions) and the geometry (ideally freestanding), also the use of cold fingers for intentional condensation of milled material far from the region of interest, as well as shadowing masks [89], can be used to help prevent the presence of FIB redeposition layers. To this end, it is important to note that, in order to optimize milling parameters and geometries, optimized SEM imaging conditions while milling are an undeniable prerequisite.

Redeposition is, thus, an issue that must be addressed when producing samples using a focused ion beam. Figs. 4-6 illustrate that the presence and location of the redeposition layer are difficult to predict, while its identification after FIB-milling may also be very challenging. We note, however, that such redeposition layers are not unique to Ga-FIBs and will also occur in all sputtering and ablation-based microtest sample processing techniques, particularly if high milling rates are used.

2.4. Mitigation measures

To mitigate physical artifacts from FIB milling, one already mentioned approach is to decrease in final milling stages the ion beam voltage [54,90,91]; for example, going from 30 keV to 2 keV was shown to drastically reduce the damage layer in silicon [57,90]. This is illustrated in Fig. 7A-C and is why in the course of FIB milling operations, it is common practice to perform final polishing steps using low milling voltage and current, in particular for TEM specimen preparation. Similarly, lowering the Ga-milling voltage from 30 to 5 kV changed somewhat the character of dislocations formed by the milling process in aluminum nanopillars; yet, this did not change significantly their mechanical response - which in turn leaves open the question of whether ion-milling did, or did not, influence their mechanical behavior [92].

Besides changing the ion energy, a substitution of the ion species also influences the knock-on damage behavior of materials. For instance, Ga ions have been substituted by inert gas ions, such as Xe [32,54,93]. This

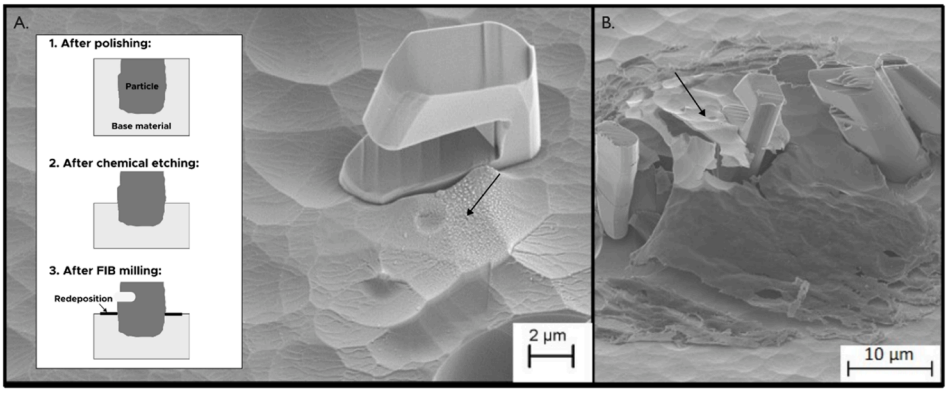

Fig. 5. (A) C-shaped bend specimen of eutectic silicon embedded in aluminum produced in Steps 1 to 3 in the inset figure. The Si particle was exposed by chemically etching the metal along a polished surface before using FIB-milling to carve a notch; (B) same region after a second etching step, revealing the thick layer of redeposited silicon that surrounds the silicon bend specimen, the presence of which is not apparent after milling in (A). Arrows highlight the same redeposited material before and after the second etching step. Micrographs by Dr. Martin Mueller, taken over the course of his thesis work at EPFL (unpublished, reproduced with permission from Dr. Mueller).

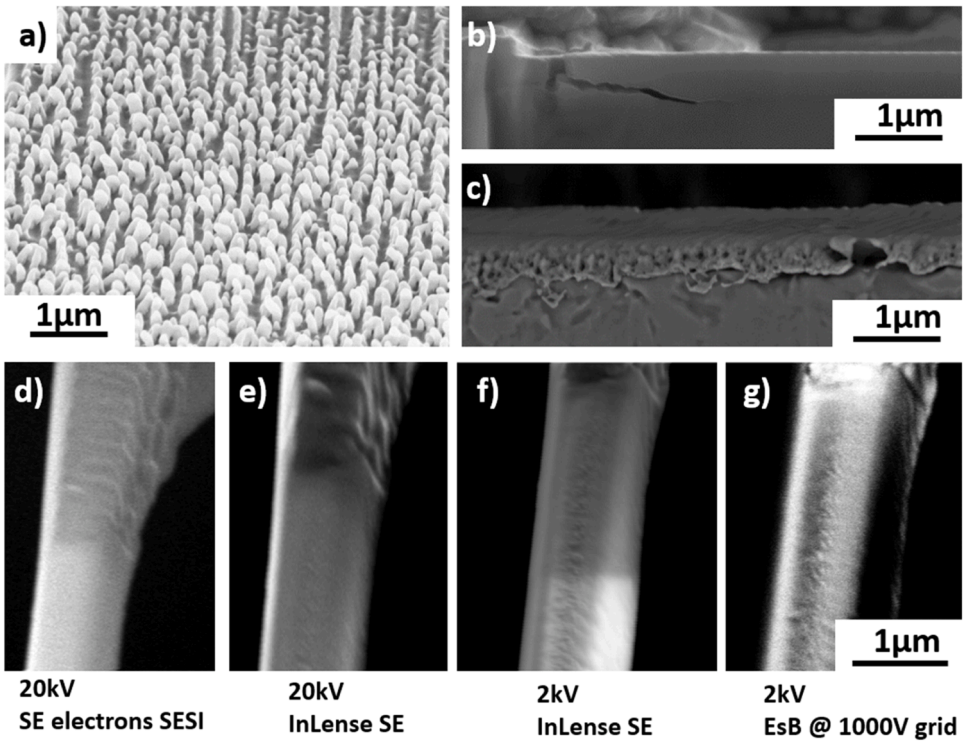

Fig. 6. Different images and stages of FIB redeposition. (a) Island growth of redeposition on a copper micro tensile specimen. (b and c) Redeposition on a steel micro fracture cantilever. The crack runs along the base-material / redeposition interface with the redeposition layer being invisible in (b) due to unfavorable imaging conditions. With optimized SEM imaging conditions, the redeposition layer can clearly be seen in (c). (d-g) A redeposition layer imaged with different (indicated) imaging conditions (Acceleration voltage (EHT) in kV, Detectors: SE=Secondary Electrons; EsB=Energy selective Backscatter @ Grid voltage of EsB). (a, d, e, f, g) Reproduced from [85] with permission from its author. (b, c) From A.K. Saxena and C. Kirchlechner, Max-Planck-Institute für Eisenforschung GmbH.

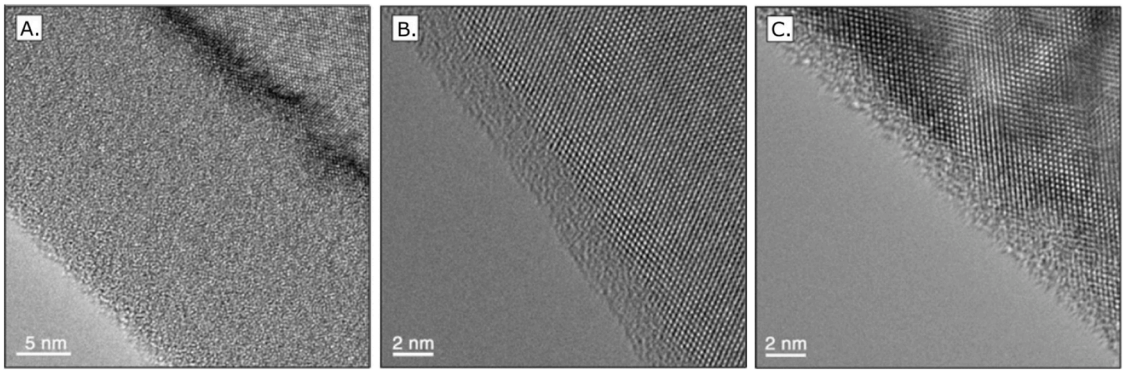

Fig. 7. Silicon lamellas FIB-milled with an incident angle of 88° and varying ion energies: 30 keV (A), 5 keV (B) and 2 keV (C). These lamellas exhibit amorphous layers of 22 nm, 2.5 nm and 0.5–1.5 nm thickness, respectively [57]. Reproduced with permission from Springer Nature.

generally shows a reduced extent of surface modification; yet material damage resulting from ion bombardment tends to persist regardless of the ion nature [34,54,94,95] (see Fig. 2). While differences in chemical interactions are indisputable for this example, also the change in atomic radius and therefore the stopping range of the high energy ions as well as the energy transfer as a function of depth are altered substantially; these effects might also make a difference in the level of artifact creation on going from one ion species to another [53,78].

Shadow milling, a method that involves the temporary masking of the region of interest, was proposed as a means to mitigate FIB damage; however, this approach has not gained widespread adoption [89,96]. Alternatively, annealing FIB-milled components has been shown to reduce the local concentration of implanted Ga ions [66,88,97] together with the level of compressive stress induced in alumina by Ga implantation [79]. Post-FIB-milling annealing is however also likely to alter the material microstructure, for example by also changing the distribution and density of dislocations or phases unrelated to FIB milling. In an extreme case, post-FIB-milling annealing was thus found to lead to the gallium-accelerated sublimation of FIB-milled magnesium micropillars [98].

Consequently, in contrast to chemically induced artifacts, which can simply not be avoided if beam ion and material atoms have a chemical affinity for one another, there are a few strategies to mitigate the impact of physically induced artifacts generated by FIB milling. It must be noted, however, that determining their relevance to the material system of interest necessitates thorough post-milling investigations, as artifact mitigation does not imply artifact elimination.

3. Influence of focused ion beam milling on microsample mechanical behavior

The aforementioned defects can significantly alter material properties. The simple fact that the thickness of the damaged layer, which can range from a few nanometers to several tens of nanometers depending on milling conditions (see Section 2.2), remains constant under specific milling conditions leads to a plasticity size effect that is entirely a result of sample preparation, given that the damaged material layer constitutes an increasing portion of the tested volume as sample dimensions decrease. More quantitatively, in uniaxial test data, the equistrain (Voigt) rule of mixtures might estimate the sample flow stress of dislocation-containing materials knowing that of the damaged surface layer and that of its undamaged core. This will introduce a near-linear dependence of the measured flow stress on the inverse of the sample diameter when the latter significantly exceeds the thickness of the altered surface layer. It should be noted, however, that Voigt́s rule of mixture likely describes accurately the effect of FIB damage only on amorphous and nanocrystalline materials that have a grain size similar to, or smaller than, the thickness of the damage layer. By contrast, in single crystals, particularly in whiskers, the quantitative impact of FIB milling on the flow stress is further influenced by the introduction of dislocation sources that can bow out and operate also in the undamaged sample core, far from FIB affected surfaces, thus altering the flow stress everywhere across the sample. The more new dislocations are introduced and the more varied they are in their lengths compared to the pristine material, the greater this effect is. Consequently, in some cases, Voigt́s rule might serve as an estimate for the flow stress of FIB milled structures, but a quantitative prediction of the flow stress of FIB milled structures comprised of a damage layer and an undamaged core remains challenging. This induced dependence of mechanical response on sample size superimposes on any size effect that might be inherent to the microscale and observed irrespective of the sample fabrication method employed [99–105].

Kiener et al. [67] have estimated the contribution of FIB-induced defects to the flow stress (τ) in copper micro- to nanoscale specimens. They contemplated a size-dependent back-stress on operating dislocation sources caused by the presence of a harder superficial layer that, in the case of copper, has been documented to exist by means of local hardness measurements along FIB-milled copper surfaces [106]. This layer was estimated to result in stress increments ranging from approximately 35 MPa for a 10 μm diameter specimen to around 110 MPa for a 1 μm diameter specimen, corresponding to ~10–20 % of the flow stresses measured experimentally [107].

The damage arising from ion-implanted dislocation loops and point defects can be considered as contributing to the flow stress through additional Taylor hardening ($\Delta\tau = \alpha G b\sqrt{\rho_0}$ [108], with G the shear modulus, ρ_0 the dislocation density, α a constant and b the Burgers vector). If one ignores initially present dislocations, this results in an increase by ~70 MPa of the flow stress if a dislocation density (ρ_0) of 2 10^{10} cm^{-2} is implanted. Likewise, Kiener et al. [67] interpreted chemical artifacts caused by accelerated ions as an additional source of solid solution [109–112] and/or precipitation hardening [113,114]. In Ref. [80] similarly sized magnesium micropillars were shown to exhibit strong differences in behavior depending on the milling sequence used, indicating a clear effect of the gallium beam on the micromechanical behavior of this metal. With a PtCuNiP bulk metallic glass, Ga ion-beam irradiation was shown to cause a brittle-to-ductile transition in the mechanical behavior of the material [115,116].

E. George, G. Pharr and coworkers conducted in 2007 investigations on the effect of FIB milling on the mechanical properties of the surface of a Mo-3at. % Nb single crystal [117]. It was found that FIB-milling hardens the metal surface and suppresses pop-in behavior during nanoindentation, leading to the conclusion that these ion-milling surface alterations could be at the origin of the observed plasticity size effect [117]. Ref. [118] stated in response that this work did not provide an adequate foundation for raising the question of FIB-induced hardening in nanopillars. Investigations were then conducted employing single-crystalline Mo rods extracted by leaching a finite length of the matrix of a directionally solidified NiAl-Mo eutectic alloy to create straight Mo single-crystalline columns that could be tested to evaluate the effect of FIB milling on the mechanical response through microcompression [101] or tensile [119] testing. Regardless of their size, leached Mo microcrystals displayed a strength of about ~9 GPa in their as-grown condition [120]. When FIB-milling was employed to thin down the outer surface of the same Mo microsamples, their mechanical behavior experienced significant alterations (Fig. 8A): after FIB-milling, tested pillars exhibited significantly lower yield strengths (~0.85 GPa) and evidenced stable plastic deformation, transitioning from a mechanism driven by dislocation nucleation to plasticity resembling that found in bulk dislocation-containing materials. On tensile testing of leached Mo fibers, Ga ion doses above 10–100 ions/nm^2 were found to reduce the strength of the fiber [119]. The deformation of these FIB-milled molybdenum pillars paralleled results of directionally solidified and prestrained pillars previously reported in [121]; yet with more scatter and variability in the flow curves than was observed in the latter after prestraining up to 11 % [101]. Similarly, clear reductions in strength coupled with alterations in the deformation mechanism after FIB-milling operations were subsequently also shown in other initially dislocation-free materials such as Ni_3Al nanocubes [122], gold micron- and sub-micron particles [123] (Fig. 8B), and more recently in square and circular pillars carved into precipitated silver cubes [103] (Fig. 8C-G). These findings highlight that microstructural signatures from fabrication techniques may significantly alter the mechanical behavior of small-scale samples and therefore must be carefully considered for reliable small-scale mechanical characterization.

The effect of FIB-milling on the mechanical behavior of 1–2 μm diameter nanocrystalline nickel pillars first produced by electroplating was investigated in Ref [124]. Lower flow stresses were measured in FIB-milled pillars compared to their electroplated counterparts; additionally, the significant tapering present in FIB-milled specimens resulted in deformation gradually progressing from top to bottom during loading. Thermal annealing of samples after FIB-milling was shown to decrease both their yield stress and the level of scatter in this quantity. Similar investigations were previously reported using sub-micron gold pillars produced by nanoimprinting and FIB-milling in Ref. [102]. Some of these pillars were monocrystalline while others displayed a few randomly oriented grains, with nanoimprinted pillars exhibiting aspect ratios in the range of 0.7–1.2. In this case, there was no discernible distinction in the flow stress characteristics observed between pillars of comparable dimensions, regardless of the production method. This observation held true for both single-crystalline and polycrystalline pillars. The scaling of flow stress relative to pillar size was reported to be similar for both methods, while nanoimprinted pillars showed evidence of twinning when their FIB-milled counterparts did not.

To address potential concerns that one might raise regarding micromechanical data from FIB-milled micropillars as a result of Ga implantation, Greer and Nix [99] reduced by half the initial concentration of Ga implanted into single-crystalline gold micropillars through argon plasma etching and, in an additional series of experiments, tested similar FIB-milled pillars that were annealed at 300 °C after ion-milling. These single-crystalline micropillars underwent compression testing, and their flow strength was compared with that of polycrystalline micropillars that were produced through templated electroplating followed by annealing, again at 300 °C, to reduce the number of grains to 2–3 grains across the pillar width. The various FIB-milled samples displayed similar size-dependent flow stresses, while electroplated samples were roughly 150 MPa stronger with a roughly similar rise in flow stress as the sample diameter decreases. These results led the authors to conclude that the plasticity size effect is not linked to the specific sample fabrication technique employed, a conclusion that was supported by 3D

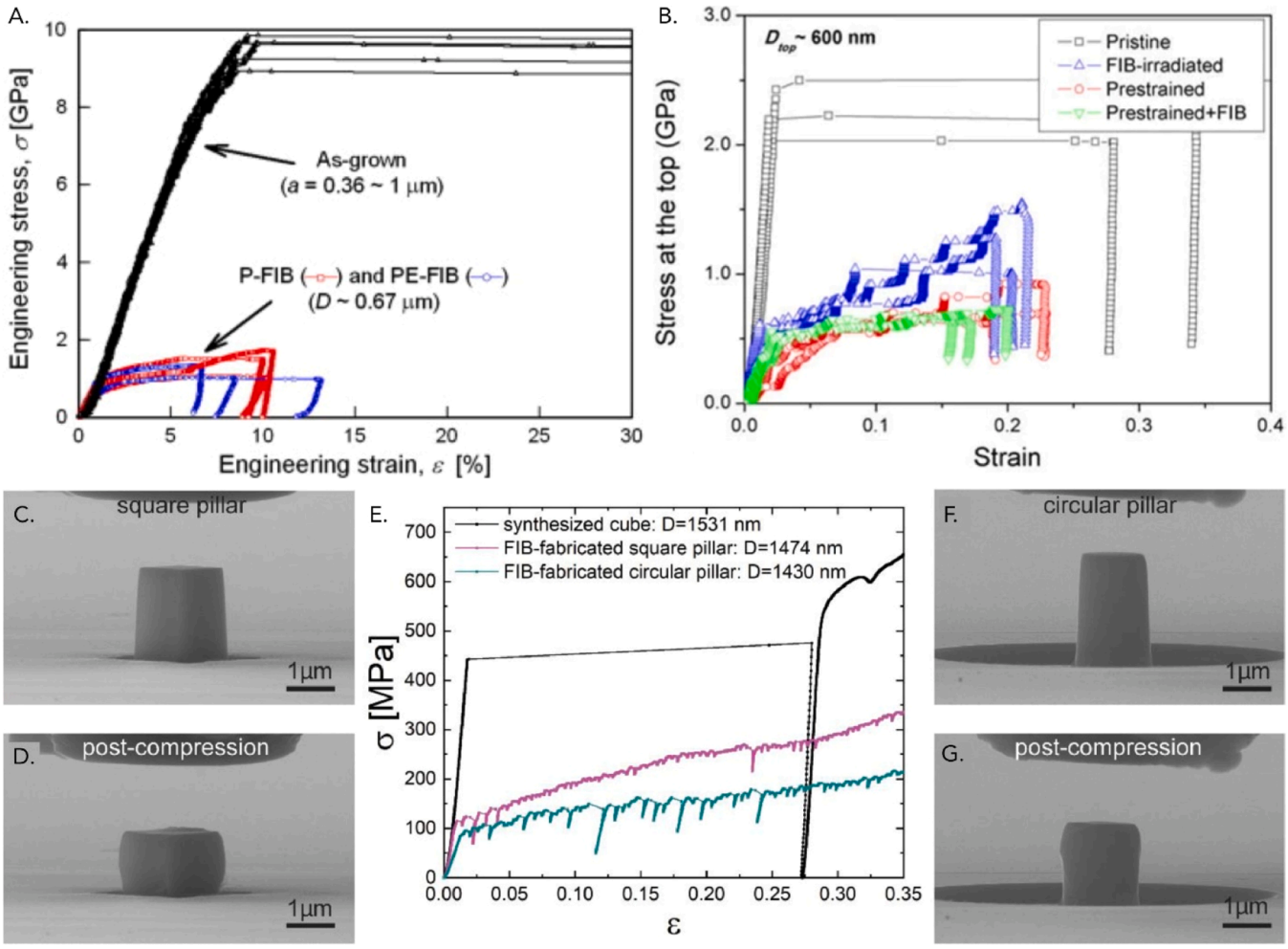

Fig. 8. (A) Stress-strain curves for Mo-alloy pillars tested in directionally solidified (as-grown) and FIB-milled conditions. The labels "P-FIB" indicate specimens polished before FIB, while "PE-FIB" denotes those that were polished and etched before FIB-milling. Reprinted from [101] with permission from Elsevier. (B) Stress–strain curves representing different gold microparticles: pristine, FIB-irradiated, prestrained, and prestrained/FIB-irradiated specimens. Reproduced from [123] with permission from Springer Nature. (C-G) Effect of FIB-milling and geometry on the deformation of synthetized silver nanocubes. (C-D) correspond to square and (F-G) to circular FIB-milled pillars before and after compression testing; while (E) displays the corresponding stress-strain curves. (C-D-E-F-G) Reprinted from [103] with permission from Elsevier.

dislocation dynamics (DD) simulations in Ref. [113].

Xiao et al. [125,126] conducted an investigation into the impact of utilizing either xenon, xenon-gallium or gallium ions in FIB milling operations that were used in fabricating 7 μm pillars of both ultrafine grain polycrystalline (UFG) and <100>-oriented monocrystalline aluminum. With UFG aluminum, regardless of the grain size, pillars fabricated with Xe ions displayed elevated flow stress levels and a somewhat more pronounced strain hardening response than did pillars prepared using Ga ions, which showed the expected weakening from grain boundary penetration by gallium (Fig. 9A-B). The higher strain hardening observed in Xe FIB pillars was linked to the larger taper angle, a consequence of the larger spot size of the Xe FIB. The *in-situ* deformation process also varied with the sample preparation method. Pillars generated using Ga primarily underwent globally homogeneous deformation featuring, however, individual grains popping out from the pillar's surface. Conversely, Xe-produced pillars exhibited a more localized deformation (Fig. 9C). With monocrystalline aluminum, the influence of ion species was less pronounced [125] (Fig. 9A-B): the Ga FIB pillars demonstrated higher levels of strength compared to their Xe FIB counterparts, a difference attributed to the greater generation of points defects and dislocation loops by Ga during the milling process. One could infer that this study shows that exposing aluminum to the gallium ion mill has the same well-known effects as exposing macroscopic samples of aluminum to liquid gallium (e.g., [47–49]).

Similar investigations designed to explore the influence of ion species on the mechanical behavior of FIB-milled microsamples were conducted in Ref. [127] through the use of FIB-milling in the fabrication of TEM dog-bone specimens from a CrMnFeCoNi high-entropy alloy (HEA). As in Refs. [125,126], xenon and gallium ions were employed and compared. Both ion types produced a comparable amorphous layer; however, significant differences, in inverse order to what was found with Ga in Al, in mechanical behavior were observed (Fig. 9D). The TEM dog-bone specimens generated using gallium FIB-milling exhibited notably higher flow stress values, reaching ~2.4 GPa, and limited deformation (~3 %), compared to their xenon FIB-milled counterparts, which had flow stresses of ~1.9 GPa and deformed up to ~20 % in tension. This difference was attributed to a propensity of gallium ions to exert a locking effect that reduces the mobility of dislocations within specimens of this nature.

Kiener et al. [128] conducted tensile tests in FIB-milled pure copper specimens oriented for single slip with side lengths ranging from 0.5 μm to 8 μm. In another study, microcast copper specimens (see below) of similar dimensions were tested in tension in Ref. [129]. While stress-strain curves in both cases displayed pronounced stress drops and the appearance of distinct glide steps on the surface, some differences in response can be noted (Fig. 10). To account for the influence of

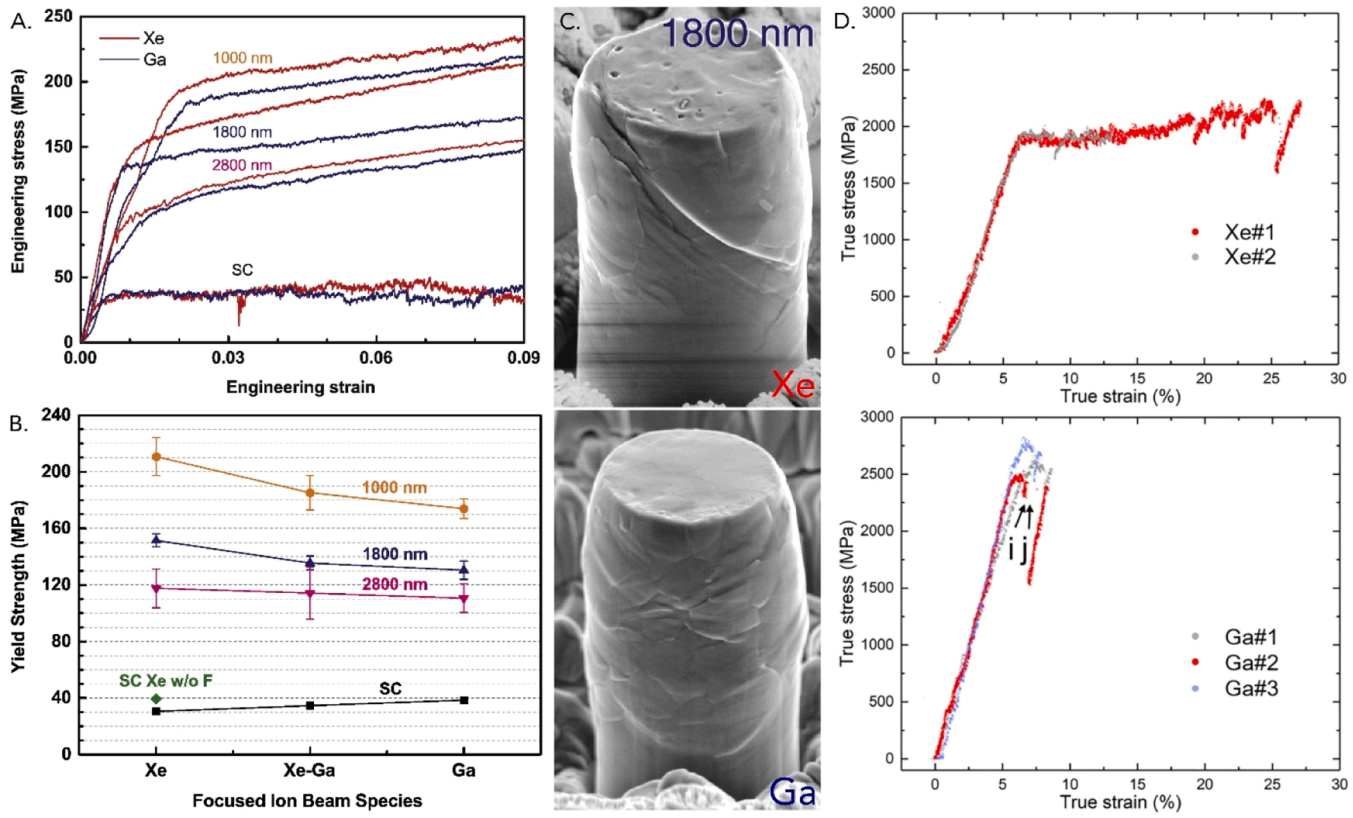

Fig. 9. Effects of ion species on the mechanical deformation of aluminum and high entropy alloys pillars. (A) Stress-strain curves of FIB-milled aluminum, comparing single-crystalline (SC) and ultrafine polycrystalline (UFG) samples with grain sizes of 1000 nm, 1800 nm, or 2800 nm, machined using Ga or Xe ions. FIB-milled aluminum using Ga or Xe ions [125]. (B) Average yield strength comparison SC and UFG aluminum fabricated by Ga, Xe and Xe-Ga FIB milling [125]. (C) Xe and Ga FIB pillars after deformation, showcasing localized and homogenous deformation along with grains popping-out, respectively [125]. (A-B-C) Reprinted from [125] with permission from Elsevier. (D) A comparison of TEM tensile stress-strain curves of CrMnFeCoNi high-entropy alloy (HEA) specimens, prepared using Xe or Ga ions [127].

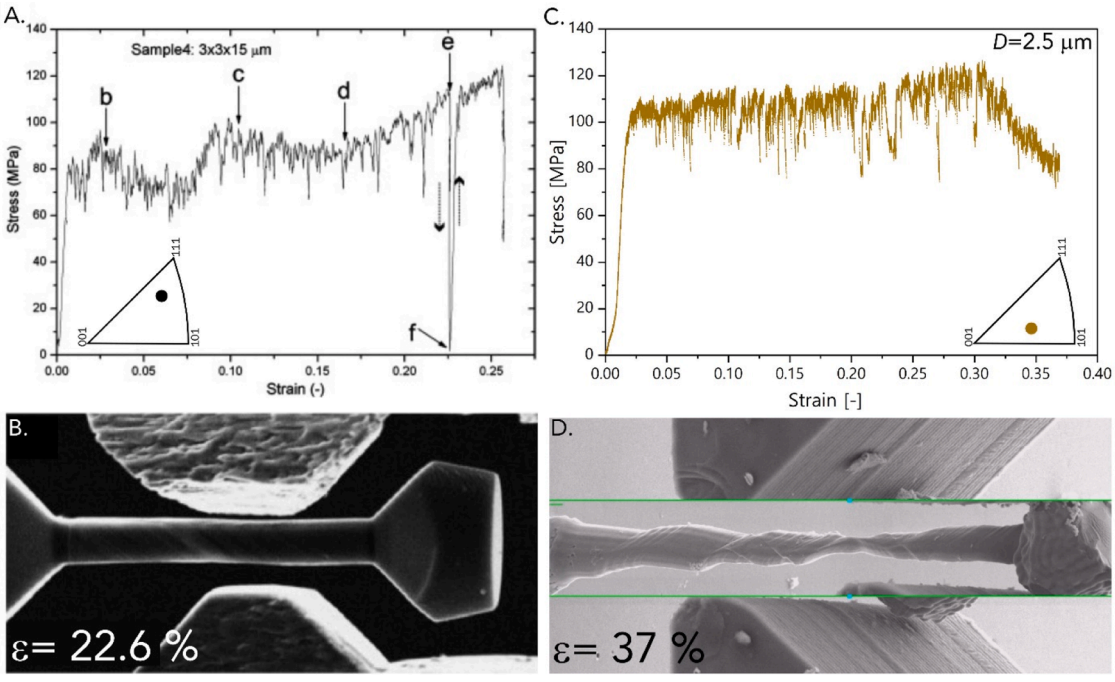

Fig. 10. Stress-strain curves and SEM images captured after deformation of *in-situ* tensile-tested copper samples produced by two different methods: (A-B) FIB-milling (Reprinted from [128] with permission from Elsevier)and (C-D) microcasting [129]. Scale in B and D is given by sample diameter given in A and C, respectively.

crystallographic anisotropy in the response of single crystals, it is necessary to calculate the resolved shear stress (τ) by using the stress (σ) and the Schmid factor (*S*) with respect to the sample's orientation, expressed as $\tau = \sigma S$. This calculation assumes that samples deform along the slip system subjected to the highest resolved stress, i.e., with the highest Schmid factor. It then becomes evident that the critical resolved shear stress (CRSS) for 3×3 μm^2 (equivalent diameter ∼ 3.4 μm) FIB-milled tensile specimens falls near 33 MPa, whereas the CRSS for microcast copper $D \sim 2.5$ μm is higher (∼48 MPa). Scanning electron microscopy (SEM) images of deformed specimens further reveal discrepancies between the deformation of these monocrystalline copper specimens, both of which are oriented for single slip (Fig. 10). The underlying cause of this disparity, whether it is to be attributed to differences in the dislocation network of the material or to the influence of surface damage associated with FIB machining, such as a hard amorphous layer, remains however to be determined.

More evidence of an influence of FIB-milling on mechanical behavior at the microscale can be found in the measurement of fracture toughness using small-scale fracture specimens. Recent reviews of microfracture testing and state-of-the art techniques can be found in [130,16,17]. Main concerns in relation with FIB-milling are related to the notch and include (i) the fact that notches, even though small, cannot always be assimilated to cracks [79,131] (though FIB-milled notches yielded reasonable K_{IC} values for Si in [132]), (ii) the development of residual stresses around a milled-notch [79], and (iii) possible (chemical and/or physical) modifications of the material around the root of FIB-machined notches.

Best et al. [133] measured the micro-sample fracture toughness of a chromium nitride (CrN) thin film produced by physical vapor deposition (PVD) and showed that the computed fracture toughness obtained from single cantilever notched beam testing varies somewhat depending on the ion species (gallium, xenon or helium were used). They also observed that pillar-splitting tests, in which cracks are initiated free of FIB-milling, yield lower toughness values than those measured in gallium FIB-milled single or double cantilever beams, and that the higher the gallium ion beam current is, the higher becomes the measured fracture toughness of the CrN thin films [133]. This influence of ion-milling on the measured toughess values was attributed to the high residual stresses that ion-milling introduces in strongly bonded solids such as this ceramic.

A similar, strong, influence of ion-milling was also documented slightly before the CrN study in another ceramic, namely single and polycrystalline alumina, which was characterized for its microtoughness using Ga ion-milled notched cantilever beams [79]. The authors documented the presence of very high residual compressive stress along the milled notch surface, of intensity 12 to 15 GPa, raising the apparent measured value of fracture toughness of alumina by 2 MPa · m$^{1/2}$.

In Ref. [134], both He- and Ga- beam milling were employed to trim excess polymer after film deposition and shape tensile specimens on push-to-pull devices. The mechanical response of the polymer films was primarily governed by the ion-irradiated edges. Both He- and Ga-FIB-milled films showed a significant stiffening compared to their bulk counterparts, with the elastic modulus increasing by up to three times. This stiffening effect was ascribed to FIB-induced crosslinking at the edges. To address this issue, researchers developed a customized push-to-pull device that allowed for precise deposition of the film on the tensile gap, thereby avoiding further FIB operations. Nevertheless, they observed that the mechanical response was also affected by the electron beam during *in-situ* TEM experiments and, consequently, they decided to conduct experiments using an optical microscope and to perform post-mortem TEM analysis. Similar to the effects of ion beam irradiation, dynamic electron irradiation present during the test can indeed have a significant impact on the materials properties. For instance, in amorphous silica, electron beam exposure has been shown to significantly reduce yield strength and induce superplasticity [135,136]. For a comprehensive understanding of electron irradiation damage, Ref. [137] offers a general overview of the topic.

In summary, there has been extensive research leading to clear evidence that the use of FIB-milling can significantly affect the surface of microsamples and the microstructure in its vicinity, and through this, influence the mechanical behavior of micromechanical structures. We next turn to alternative strategies designed to either exclude FIB milling entirely, or use it while nonetheless testing regions of material unaffected by its use.

4. Alternative strategies

FIB-milling is not a necessary step in the production of shaped microsamples for mechanical testing: there are now many other microfabrication techniques that produce small-scale structures suitable for mechanical testing of material that has not been irradiated by a focused ion beam.

One approach that has already been mentioned is to extract, by leaching, a conveniently shaped phase from a two-phase material. For uniaxial testing, the minor phase of a rod eutectic is ideal in this regard. This approach was used by Bei et al. who solidified a eutectic alloy directionally in a Bridgman furnace, varying the microstructural scale by varying the cooling rate during solidification [120,121,138]. After directional solidification, a polished surface normal to fibers in the eutectic alloy was immersed in an etchant that selectively dissolves the matrix, leaving behind individual fibers as freestanding rod-shaped microsamples of controlled diameter and suitable for mechanical testing. Monocrystalline molybdenum pillars ranging in diameter from 360 to 1400 nm extracted from a NiAl-Mo alloy were produced by this method and tested in compression [120,121,139] or in tension [119] (Fig. 11). Pristine Mo fibers exhibited mechanical properties similar to defect-free whiskers, which were strongly altered if the density of dislocations within these pillars was raised by subjecting the long composite to deformation before the etching process. Similarly, monocrystalline aluminum and beryllium fibers were produced in Refs. [140,141] through selective etching of an Al/Al_2Cu or an Al-2.4 at.% Be eutectic alloy, respectively (Fig. 11). The yield strength of these fibers in tension evidenced an influence of both the cross-sectional area and the density of dislocations in the fiber. While this elegant approach has produced valuable studies on microplasticity, it does have limitations in terms of both shape and composition, given that it is restricted to the rod or plate phase of eutectic or near-eutectic alloys.

Sample production for the mechanical characterization of small-scale structures has also benefited from manufacturing techniques commonly available in cleanrooms, particularly those derived from the semiconductor industry. These include lithography, deep reactive ion etching (DRIE), and thin film deposition. Lithographic cleanroom processes generally begin by the application of a photoresist layer onto silicon (i.e., through spin coating) and continue by selectively etching the desired shape from the resist by means of exposure (i.e., photolithography, X-rays, electron beam) and development steps. Once the photoresist has been developed, the pattern is transferred onto the hard mask and silicon wafer, the latter typically using the DRIE process to etch deep features; this process involves periodically switching between gases to alternately etch and protect the surface, commonly utilizing SF_6 and C_4F_6 plasmas (Fig. 12A). This approach enables the direct production of silicon pillars for compression testing, as demonstrated in Refs. [142–144] or of GaAs pillars [145]. These pillars demonstrated remarkable strengths compared to their FIB-milled counterparts, attaining values that closely approach the theoretical limit. Moreover, they display increasing levels of plasticity as the pillar diameter decreases [142]. One should note, however, that etching under a mask may damage the sides of the specimen to some extent and the nature of the damage will depend on both the gases employed and etching conditions.

By combining lithography and subsequent deposition of material onto the etched substrate, it is furthermore possible to create intricate two-dimensional patterns and structures on a substrate and thus to test

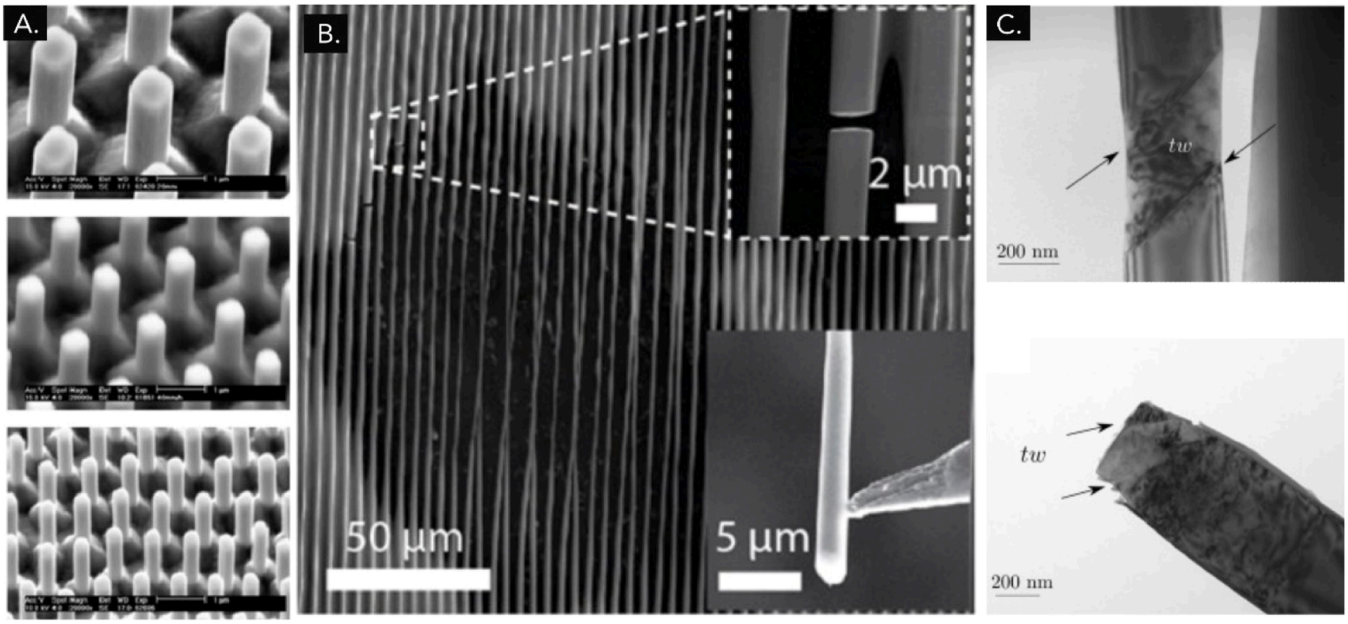

Fig. 11. Structures fabricated by directional solidification and selective etching. (A) Set of Mo-pillars with different diameters. Reprinted from [120] with permission from Elsevier. (B) Aluminum fibers. Reprinted from [140] with permission from Elsevier. (C) Beryllium fibers evidencing twins (tw) after *in-situ* TEM tensile deformation. Reprinted from [141] with permission from Elsevier.

properties of thin films. Testing thin films deposited on substrates using microfabrication processes dates back to the early 1960s [146], where polymers or halite substrates were employed. The semiconductor industry later triggered the incorporation of silicon substrates and silicon-based micro-electro-mechanical systems (MEMS). For instance, gold and silica (SiO_2) cantilever beams 1 μm thick have been produced and tested using a nanoindenter [147] (Fig. 12C), while tensile tests of freestanding copper, nickel, silver as well as titanium and aluminum thin films on silicon are reported in Refs. [148–151]. The literature on thin films in now extensive and includes the use of other substrates [152,153].

MEMS technology has also found direct application in the uniaxial testing of thin film materials [154,155]. For instance, Sharpe et al. [156] measured the Young's modulus of polysilicon films 1.5 to 3.5 μm thick by means of tensile testing. Haque et al. [157] measured the properties of ultra fine grained (UFG) aluminum thin films deposited on silicon substrates through tensile testing, employing silicon beams on the side to measure displacements (Fig. 12D). Additionally, by combining interferometry and compression, the tensile behavior of gold, copper, and aluminum films of varying thicknesses was characterized in Refs. [158,159], to produce data that exhibit clear signs of a plasticity size-effect.

In addition to evaporation and deposition techniques, electroplating can also be used to fill patterns etched by lithography into photoresist layers (a process often called LIGA) [160–165,100,166], or into cylindrical cavities produced by anodic aluminum oxidation [167]. Here, etched patterns are submerged in an electrolyte, metal ions are electrochemically deposited onto the exposed areas of the conductive substrate and, finally, the resist is removed, leaving behind fully 2D shaped dense metallic microstructures (Fig. 13). This process typically yields nano-twinned or nanocrystalline structures, which can be subsequently annealed to produce monocrystalline samples [100,168,164,169,165]. Gold and copper specimens containing dislocations, of diameter down to 25 nm, have been tested both in tension and compression, exhibiting localized deformation and strong size-effects [164,165,168]. As mentioned above, the effect of FIB-milling on nanocrystalline nickel produced by electroplating was explored in [124]. Patterned electroplating also enables the fabrication of more complex architectures such as three dimensional copper lattices, gold helices and nickel microsprings [170–172] (Fig. 13D-F). Copper lattices thus produced to have a relative density of 0.8 have demonstrated strength levels significantly outperforming those of monolithic bulk copper.

Hot embossing, also called nanomolding or nanoimprinting, is the process of reproducing a design shaped as a hollow within a die made of a material sufficiently hard to deform the (generally solid) material that is to be shaped by driving it under applied stress to fill the hollow, much as in the traditional processes of closed-die forging or coining; recent reviews of this class of processes are in Refs. [173,174]. For metals, this fabrication technique relies on the plastic deformation of soft and ductile metals or alloys into a structured rigid die or, at smaller size scales and higher temperature, on diffusion, while for amorphous materials this is made possible above the glass transition temperature by viscous flow [173]. Micropatterned silicon, produced via lithographic processes as previously described, has been employed as a hot-embossing die to create sub-micron structures using silver, gold, and a gold-tin alloy [102,175–177]; however, other materials such as anodized aluminum oxide or silicon carbide have also been found to be suitable [173]. In an elegant method, an anodized aluminum oxide template was filled with a bulk metallic glass, the other side of which was infiltrated into a steel wire mesh that enabled tensile removal of the molded nanowire arrays from the alumina die [178]. Essential forming parameters to achieve complete cavity filling are vacuum conditions, applied forces, temperature, and surface conditions. For instance, a gold interlayer was deposited to improve wettability before embossing a molten gold-tin alloy at 320 °C [177]. Similarly, when imprinting pure silver or gold into silicon, the process was carried out under high vacuum conditions and at 400 °C, with mechanical pressures reaching up to 300 MPa. As the metal embossing process typically takes place at temperatures exceeding the recrystallization temperature of the embossed metal and involves substantial deformation, it facilitates the fabrication of monocrystalline metallic microstructures. Once filled, silicon dies can be selectively etched in a potassium hydroxide (KOH) water-based solution, leaving metallic pillars attached to bulk metal (Fig. 14). Microcompression tests conducted on silver pillars that were produced in this manner, with diameters ranging from 130 to 3000 nm, reveal a transition from bulk to dislocation-nucleation governed plasticity [179]. The mechanical

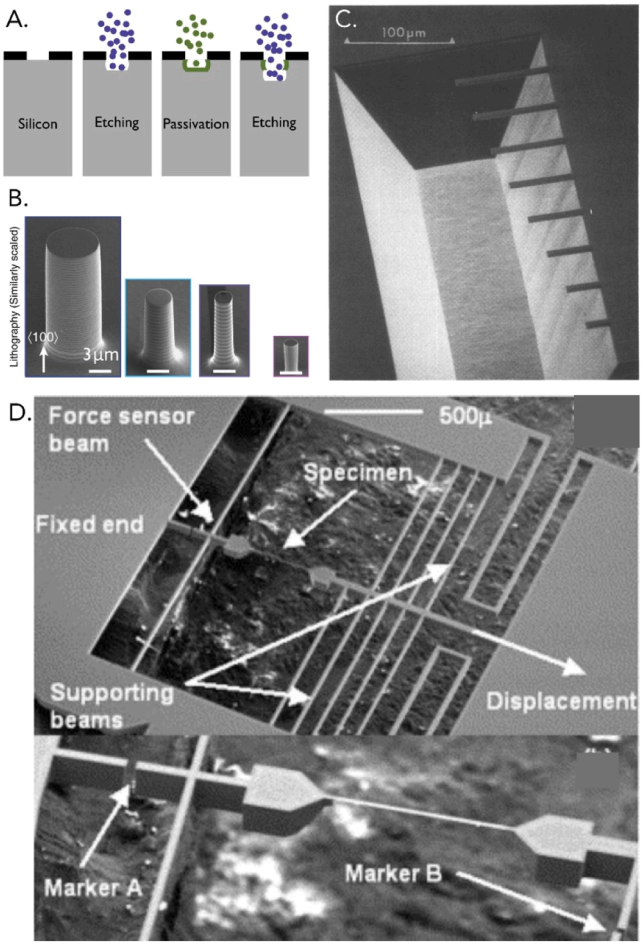

Fig. 12. Microstructures obtained by silicon microfabrication techniques. (A) Schematic illustration of the deep reactive ion etching steps (DRIE). (B) Lithographically obtained silicon pillars [142]. (C) Thermally grown silica (SiO_2) cantilever beams produced by etching both the silica and the silicon substrate. Reproduced from [147] with permission from Springer Nature. (D) Microfabricated tensile test chip showing a free standing aluminum film specimen; the difference between Markers B and A gives the elongation of the specimen. Reprinted from [157] with permission from Elsevier.

behavior of nanoimprinted gold pillars was compared with their FIB-milled counterpart in Ref. [102] (see Section 3).

The use of silicon microfabrication for the production of embossing dies enables rapid and scalable prototyping while allowing for straightforward customization of dimensions and aspect ratios. Capabilities of nanoimprinting are, however, somewhat constrained when it comes to complex geometries, particularly those with intricate, expansive designs, because achieving complete filling can be quite challenging. Additionally, nanoimprinting requires materials that exhibit low-pressure, low-temperature flow characteristics coupled with chemical compatibility with the die material, which restricts the material selection.

Microcasting is a downscaled version of another old metallurgical process, namely casting, adapted to fabricate dense metallic microstructures in various complex shapes. Microcasting is, like casting, generally composed of three stages, namely (i) mold manufacturing, (ii) casting of the molten metal, and (iii) demolding. A schematic illustration of the process is shown in Fig. 15A. Metal casting at the microscale is most often conducted through pressure infiltration, meaning by forcing mechanically the melt into the mold, because one must generally overcome capillary forces, which play a strong role at this scale and generally oppose ingress of the melt into the mold. After solidification and to avoid deforming the micrometric structures thus produced, demolding is generally accomplished through selective etching, wherein both the mold and the cast metallic component are immersed in an etchant that selectively dissolves the mold.

There are several available microcasting mold manufacturing processes. In Refs. [180–184], a miniaturized version of lost-pattern investment casting was demonstrated. Polymeric patterns of the part to be cast are immersed in a ceramic slurry (also known as investment) to replicate its external form in the surrounding shell. Following a drying process, the investment undergoes sintering, while the pattern is removed by oxidative pyrolysis. The properties of the investment compound significantly affect the resulting casting surface roughness; in particular, any polycrystalline mold will, after heating (e.g., to sinter the investment compound, or to prevent metal solidification during infiltration of the mold) feature along its surface a groove wherever the surface intersects a grain boundary. This causes depressions on the mold surface that are later replicated along the surface of the (generally pressurized) cast metal. This leads to the formation of surface defects that go unnoticed on macroscopic castings but are, at the scale of a microcasting, unacceptable. Because of that, monocrystalline or amorphous molds are best used.

Precise molding for the production of long cylindrical samples has been achieved using microstructured silica capillaries [186], or by growing monocrystalline NaCl crystals around organic patterns while slowly evaporating a slightly undersaturated water solution and then removing the organic pattern by pyrolysis [104]. More specifically, monocrystalline NaCl molds have been produced to contain long and smooth hollow cavities formed from pyrolizable (polymeric) fibers. These enabled the casting of aluminum or magnesium wires of diameter down to 7 µm, with a surface roughness of around 50 nm [104,187–190] (Fig. 15B). More recently, a method was introduced in Ref. [191] employing resins loaded with salt particles to fabricate easily leachable structures by 3D printing, in turn enabling the production of molds for castings having geometrical features defined down to 100 µm. This technique has been used to produce aluminum and magnesium lattices.

It is also possible to achieve micron-scale molding through femtosecond laser machining followed by selective etching of fused silica substrates, as demonstrated in Ref. [185,192] (Fig. 15C). This method offers the major advantage of enabling the production of essentially any fully 3D freeform shape provided it is continuous, with features defined down to roughly 1 µm precision. Another advantage of the method is that the mold is carved into an amorphous, i.e., grain-boundary-free, material. It has been implemented with silver, copper, gold and their alloys, to fabricate structures ranging in size from a few millimeters down to the micrometer scale. Alternatively, lithographically patterned silicon substrates, coated with an outer layer of oxide, have been produced to cast copper and silver mushroom-like structures amenable to tensile testing [105,129,193,194] (see Fig. 1 of Ref. [129]). The use of silicon microfabrication techniques for precise molding offers outstanding dimensional control while enabling the parallel fabrication of many components; however, being based on silicon lithography, this molding method is more limited than femtosecond laser glass mold micromachining in terms of the geometries that it can produce.

Typically, microcast metals have a grain size that largely exceeds that of features of the microcasting, such that individual castings are monocrystalline or contain only a few grains. Common features of the plasticity of microcast metal tensile bars are therefore a combination of single-crystal deformation with phenomena characteristic of small-scale plasticity; these include large shear deformation along glide planes of highest resolved shear stress, an orientation-dependent work hardening rate, a distinctive jagged stress-strain response with frequently visible slip steps, and a raised flow stress that increases with decreasing sample diameter [104,195].

Micromolding techniques, whether they use solid or liquid metal, offer the potential for achieving micro- or nanometric resolution. Both can, however, face issues related to the metal's chemical reactivity,

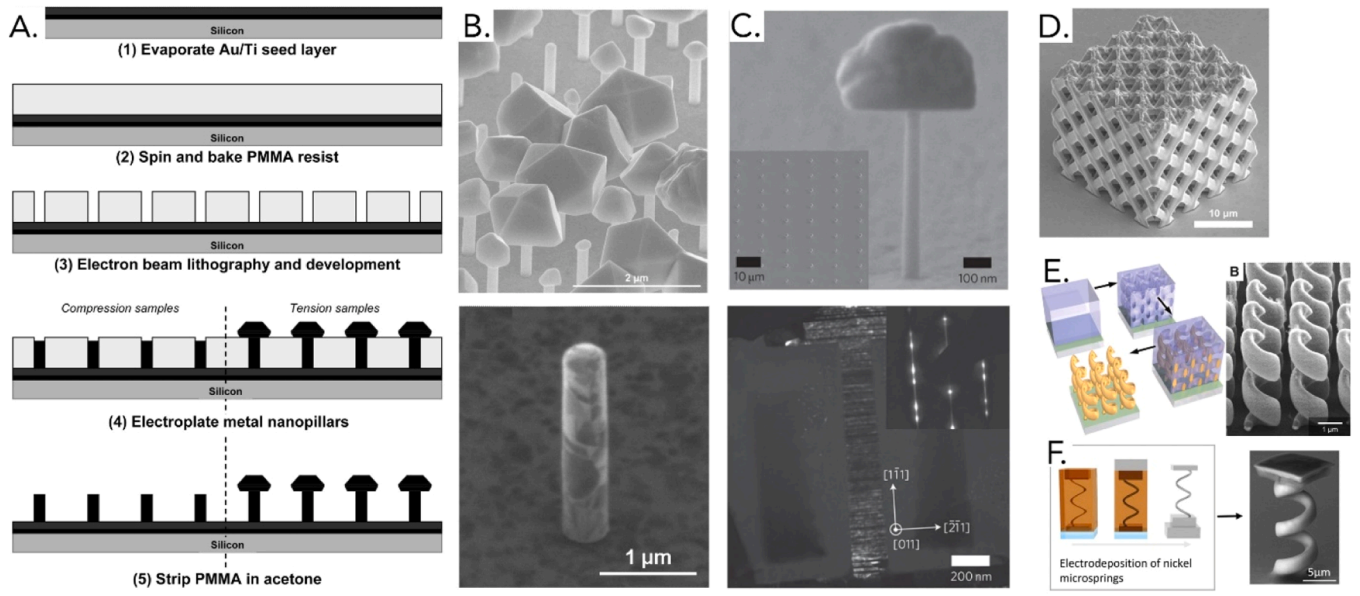

Fig. 13. Template-assisted electroplating techniques. (A) Schematic illustration of e-beam lithography in combination with electroplating. Reprinted with permission from [164]. Copyright 2010 American Chemical Society (B) Mono- and nanocrystalline copper pillars produced as illustrated in (A). Adapted with permission from [164]. Copyright 2010 American Chemical Society. (C) Electroplated nanotwinned Cu wire for tensile testing. Reproduced from [169] with permission from Springer Nature. (D) SEM image of a copper microlattice with octet geometry. Reprinted from [170] with permission from Elsevier. (E) Schematic illustration of the process and a lateral image of gold helix structures. From [171]. Reprinted with permission from AAAS. (F) Electrodeposition of nickel microsprings. Reprinted from [172] with permission from Elsevier.

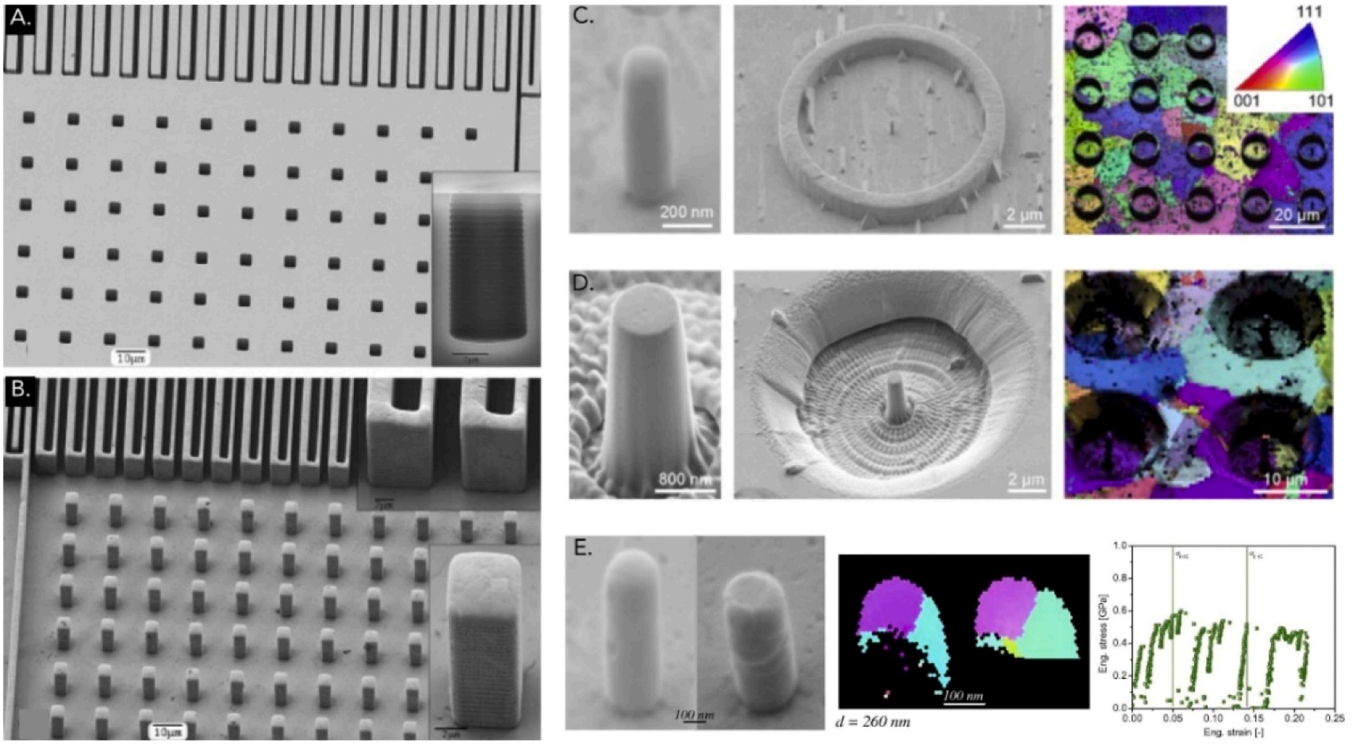

Fig. 14. Hot embossing: (A) Microfabricated silicon mold and (B) silver pillars after hot-temperature embossing and mold dissolution Reprinted from [175] with permission from Elsevier. (C-D) SEM images and EBSD analysis of a (C) hot-embossed and (D) FIB-milled gold pillar [102]. (E) Microcompression response of a hot-embossed polycrystalline gold nanopillar [102]. (C-D-E) Reprinted from [102] with permission from Elsevier.

which can appear during either the mold infiltration or mold dissolution phases. When utilizing silica or silica-coated molds, the metal must only contain elements that have an oxide less stable than that of silicon; otherwise, unwanted reactions are likely to occur along the mold/metal interface. Moreover, demolding at this scale presents its own set of challenges since mechanical methods are likely to damage the produced small-scale, and hence delicate, microcastings. Chemical approaches, such as the use of hydrofluoric acid to dissolve silica or KOH for silicon, work with some metals, but also narrow down the available options, as the metals intended for casting must remain inert during this stage.

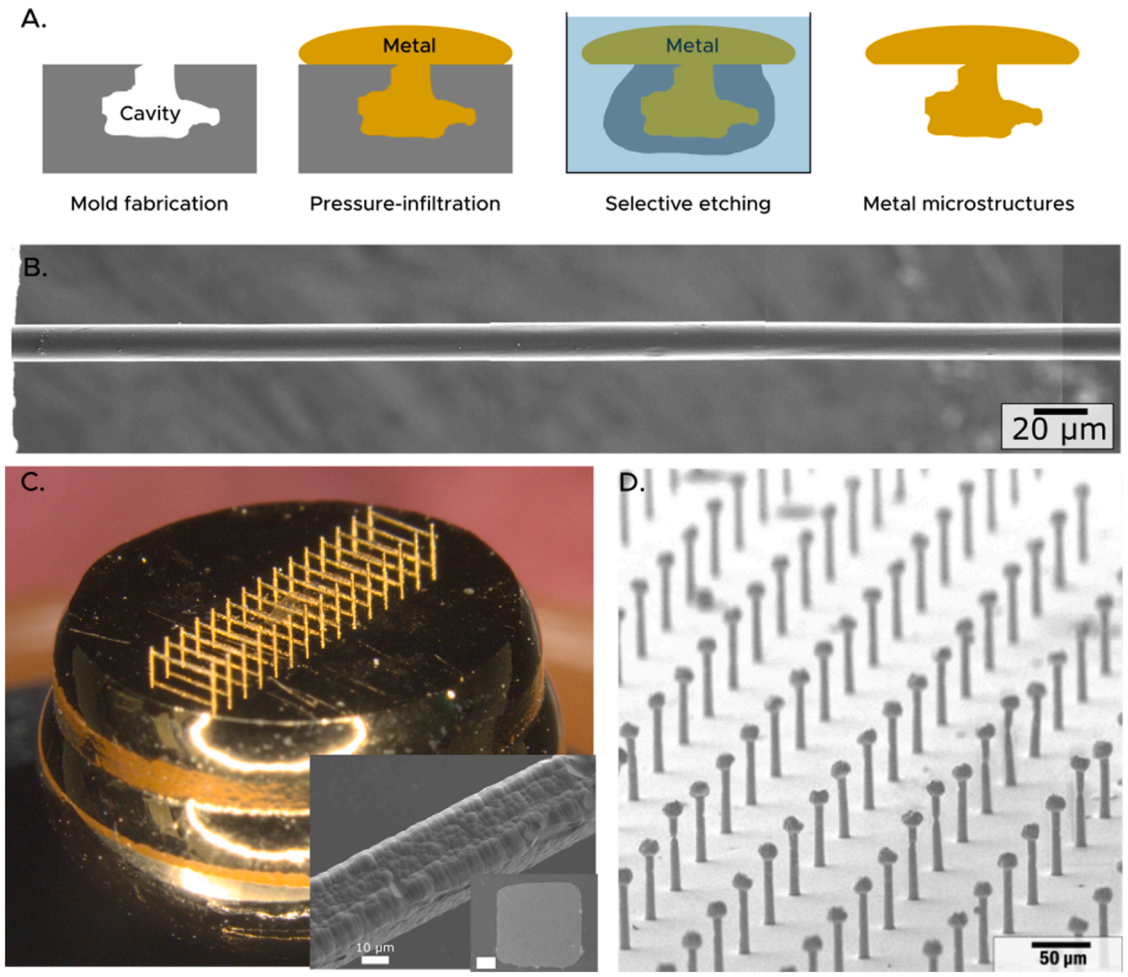

Fig. 15. Microcasting: process and resulting as-cast structures. (A) Schematic illustration of the microcasting stages. (B) Aluminum wire with a diameter of approximately 15 μm and a length of 1 mm produced using single-crystalline NaCl molds grown around nylon fibers. Reproduced from [104] with permission from Springer Nature. (C) Gold beams produced using a femtosecond laser micromachined silica mold. These structures have an H-shape configuration, each segment has a cross section of 50×50 μm^2 and the middle segment has 1 mm in length. SEM images (inset) reveal the surface roughness associated with laser micromachining and the fully-dense cross section of the metal within the casting [185]. (D) An array of microcast silver tensile test specimens, each with a diameter of approximately 13 μm, produced using a microfabricated silicon mold [105].

While salt molds exhibit relative stability against metals and readily dissolve in water at room temperature, their drawback lies in the relatively low melting point of NaCl (801 °C), which falls below the melting temperature of many engineering metals; also, its comparatively high vapor pressure at elevated temperature can cause problems in processing.

Common to processes of nanoimprinting and microcasting is the influence of thermal mismatch stresses, which arise from differences in the thermal expansion coefficient between the mold or die on one hand, and the metal on the other, coupled with the significant temperature excursion experienced by the mold/casting assembly during cooldown from (elevated) processing temperatures. Resulting thermal stresses are typically relieved through the emission of dislocations, and thus lead to the incorporation of geometrically necessary dislocations into the samples. This thermal dislocation density is scale-dependent [105], and thus creates another source for plasticity size effects in the form of an increased yield stress with decreasing sample size.

Yet another approach for the production of micro- or nano-scale test samples is to test directly synthetized samples, often grown from the vapor or precipitated from a solution, and taking the shape of particles [103,122,123,196–204], or whiskers (at times also called nanowires). Elongated whiskers produce a sample geometry amenable to testing that has probably been the first successful microsample fabrication technique [205–209]. Ref. [210] provides a review on the synthesis of silver nanoparticles. To name a few examples, Wheeler et al. [201] studied the deformation at room and elevated temperature (up to ~500 °C) of gallium nitride (GaN) prisms grown by metalorganic vapor phase epitaxy. References [198–200] employed synthetized silver nanocubes to study the dynamic response when those, propelled by laser-induced projectile impact testing (LIPIT), hit a material at very high velocities, while Ref. [103] focuses on the quasi-static micro-compression behavior of these silver nanocubes.

In recent years, there has been a remarkable surge in the advancement of freeform additive manufacturing techniques. This has opened up the possibility of 3D printing a wide range of materials, including polymers using two-photon polymerization [211–216], composites [217–219], pure silica [220,221] or other oxides [222–225]. Metals too can be 3D printed. Most emerging processes that directly write metal to produce structures at the micro and/or nanoscale operate either by depositing nanoparticles embedded within a matrix or by reducing metal ions within a solution [226–239]; an in-depth review can be found in Refs. [240,241]. One significant advantage of these techniques is that they are mostly one-step fabrication processes, often coupled to a multiscale capability. A notable general challenge in metal 3D printing is the wide variation in surface roughness and often also the microstructure obtained, due to the progressive point-by-point and/or layer-by-layer

assembly of components, with each resulting microstructure potentially featuring a unique distribution of defects (Fig. 16). While the list of available techniques continues to grow, we highlight approaches based on electrodeposition for mechanical characterization due to their ability to yield smooth and dense structures. Refs. [242] stands as a noteworthy illustration of this, wherein copper micropillars were fabricated using a localized electroplating technique introduced in Ref. [226] (Fig. 16C&F-G) to investigate the effect of strain rate and grain size on the compressive behavior at the microscale.

Another approach for the micromechanical characterization of materials free of material modifications induced by ion beams is to use FIB-milling to produce and test samples having a geometry such that the most highly stressed regions fall outside those where milling was used. In Refs. [243–247] a combination of chemical etching and FIB-milling was used to test the local, microscale strength of brittle materials, namely alumina, silicon and silica. In Refs. [243–246], micrometer-sized particles or fibers embedded in a metallic or polymeric matrix were first exposed by preferential chemical etching and were subsequently

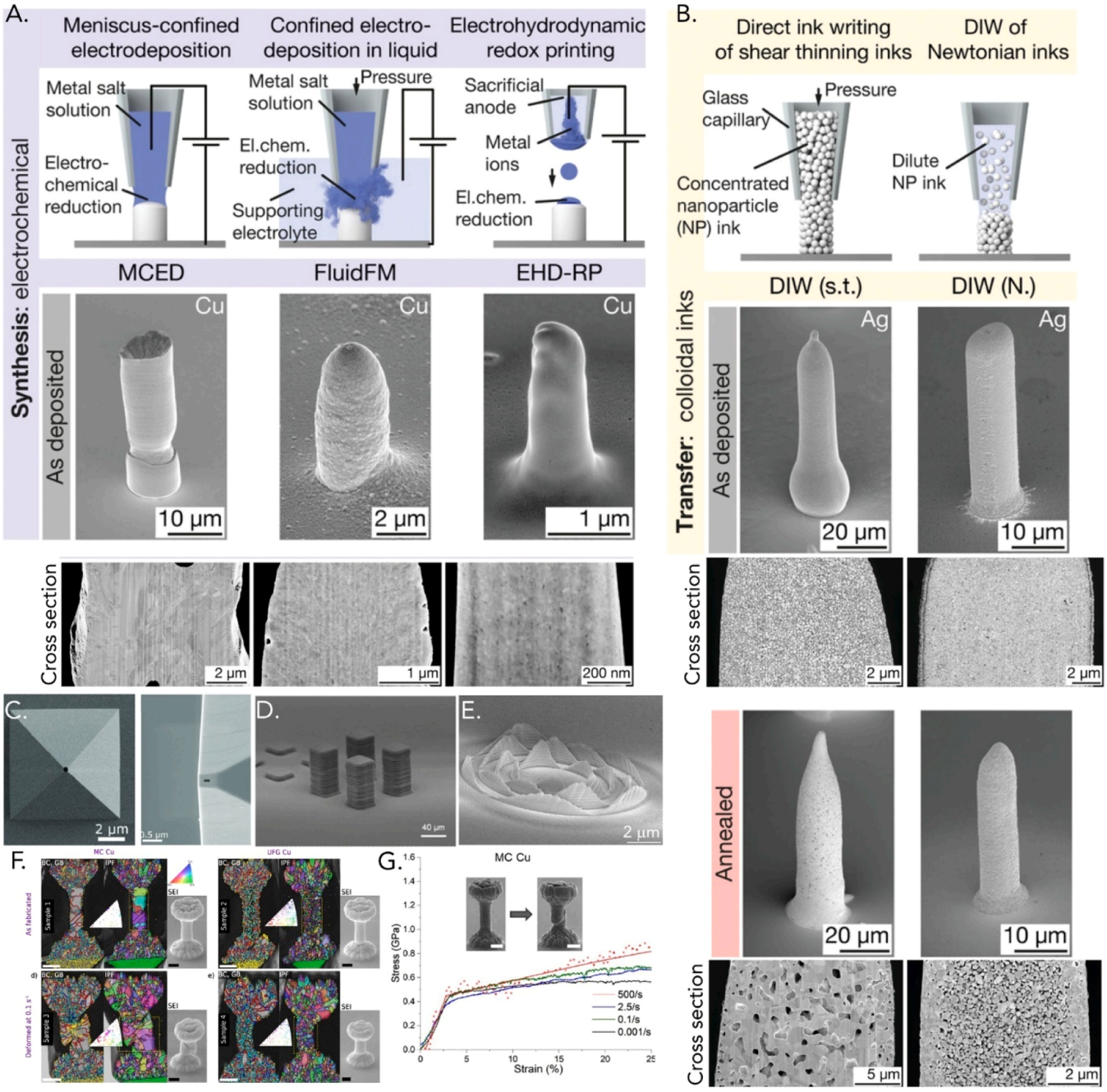

Fig. 16. Metal 3D-printed structures: (A) Copper pillars printed by an approach based on electrochemical synthesis and the corresponding cross section. Copyright 2020 Wiley. with permission from [241]. (B) Silver pillars printed by direct ink writing and the corresponding cross section, before and after annealing. Copyright 2020 Wiley. Used with permission from [241]. (C) Smooth pyramids with different tip apertures produced by electroplating of locally dispensed ions in liquid through a hollow atomic force microscope cantilever (FluidFM in (A)). Copyright 2020 Wiley. Used with permission from [226] (D) Square micropillars printed by laser direct-write of silver nanopastes. Copyright 2010 Wiley. Used with permission from [239]. (E) Concentric waves printed by electrohydrodynamic redox 3D printing (EHD-RP in (A)) [236]. (F) Microcrystalline (MC) and ultrafine grain size (UFG) copper pillars, produced by electroplating of locally dispensed ions in liquid, before and after quasi-static and high strain rate compression with the corresponding EBSD maps [242]. (G) Stress-strain response of MC copper pillars shown in (F) at various strain rate values [242].

notched using FIB-milling to create micromechanical test samples having the shape of a "C", Fig. 17. These were then tested by applying a compressive force that closes the "C", this in turn leading to the build-up of high tensile stresses in the region along the external surface of the C-shaped sample, which was exposed by etching but did not experience ion-milling.

Alternative strategies in this vein include bend-testing, over a FIB-milled cavity in the metallic matrix, of silicon particles solidified within an Al casting alloy [247]. These were also exposed by leaching the Al matrix and were then milled along their sides leaving the flat, initially facetted, tensile face unaffected by FIB-milling. To minimize the influence of FIB damage on the measurements, the samples were shaped with a trapezoidal cross-section in such a way that tensile stresses in the lower face of the sample are developed away from the milled edges. Similarly, the test specimen geometry was adapted in the testing of cantilever beams designed to measure the interfacial strength between silica and iron, in a way that ensures that peak interfacial stresses along the interface do not fall within the FIB-milled region; this was achieved by means of small notches placed at the sides of the cantilever beams [248].

A limitation of this class of micromechanical tests is that they are often less rich in the data they provide, given that they so far only measure the local strain (and if the deformation law is known the stress) at rupture of the material – this is unlike tests conducted using uniaxial tension or compression samples, which give the entire deformation law prior to failure. To produce measurements of the small-scale local deformation law, one would have to devise methods for the simultaneous measurement of stress and strain within, and only within, the highly stressed tensile region in a sample that features strain gradients– this, although now doable in principle (e.g., by a combination of image analysis and diffraction), has to our knowledge so far not been reported.

FIB-milling to produce samples that are tested outside of FIB-affected regions can also be used to produce microscale fracture toughness measurement samples containing sharp cracks that are free of FIB-damage. Proposed strategies include taking advantage of pre-existing cracks or defects by milling micron-sized samples around those [249] or the introduction of cracks before or at intermediate steps during the micro-sample preparation process, e.g., by nearby indentation at high loads [250]. Pillar-splitting has been proposed to measure the resistance to crack propagation in microscale samples without the need to precrack the specimens [251]; however, results may still be affected by FIB milling if the pillars are produced with this technique and their diameter is not sufficiently large [252]. Alternatively, a number of sample geometries have been proposed that do use FIB-milling but carve specimens designed to produce stable propagation of a (sharp) crack, allowing the determination of material properties away from the FIB-affected regions. These include double cantilever beams [132, 253–255], clamped beams [132,256–259], chevron-notched single cantilever beams [260,261], and a single cantilever delamination geometry recently proposed to measure the fracture toughness of interfaces [262] (Fig. 18). On occasions, pre-fatiguing the notch has also been used to initiate stable crack propagation in fracture toughness

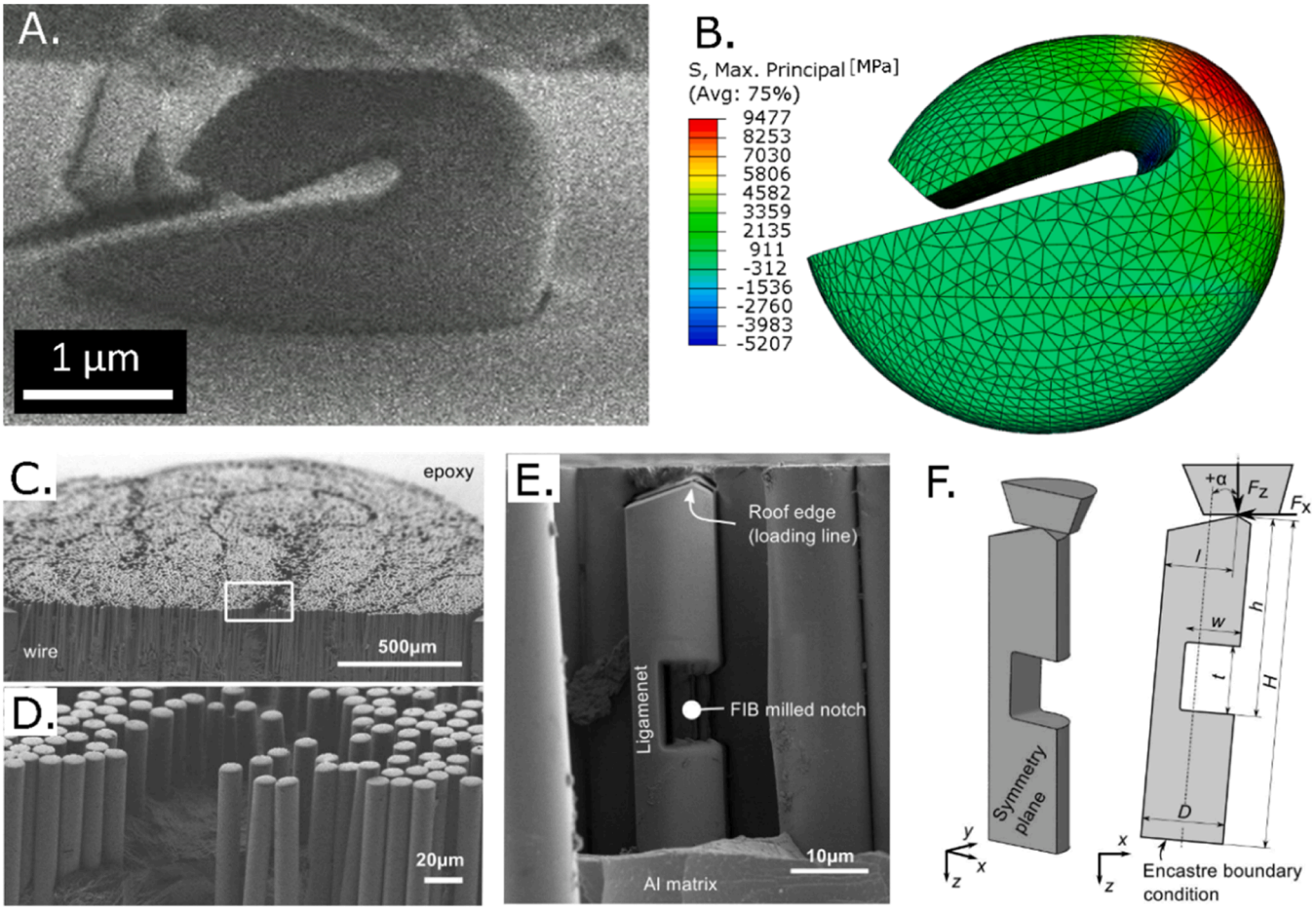

Fig. 17. (A) In-situ micromechanical testing of C-shaped silicon oxide particles, the notch of which is FIB-milled, and (B) finite element model of the test showing that maximum principal stresses are located in the external surface of the particle, away from FIB-milled regions [246]; (C-F) show a notched specimen prepared in an alumina fiber, in (C) a composite wire containing the alumina fibers is observed with low magnification while in (D) the fibers, after chemical etching of the aluminum matrix, are observed at higher magnification. (E) shows a notched fiber prepared by FIB-milling. (F) shows a sketch of one-half of the notched specimen and its dimensions [243].

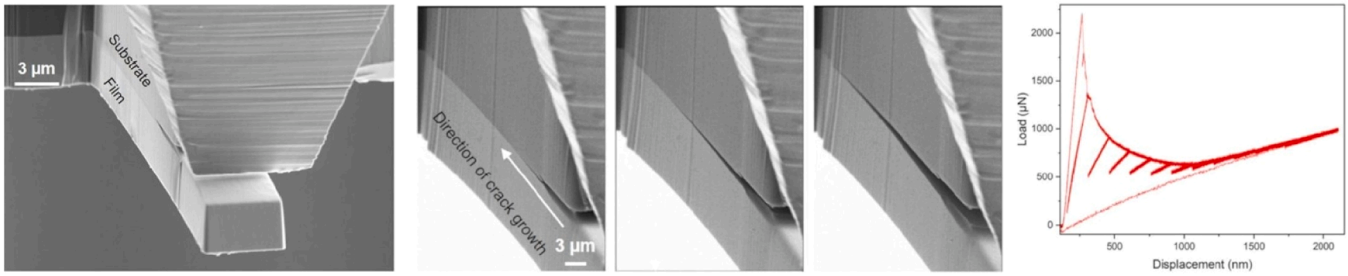

Fig. 18. Cantilever delamination geometry and stable crack growth propagation during *in-situ* SEM testing [262].

microspecimens [24].

Finally, in the context of small-scale characterization techniques that exclude FIB-milling artifacts, it is pertinent to mention nanoindentation as an alternative, even though it is not the intention of this review to cover the method. Readers are referred to the extensive body of literature on this topic [263–268] or to a few extensions of the method to high strain rates [269,270], high temperature [271,272], embedded particles [273] or the production of nanoindentation maps [274].

In summary, it is evident that, unlike the near-universal FIB approach, the various alternative microfabrication strategies discussed in this section are highly material-specific. Each technique, in addition, potentially imparts a unique microstructural signature reflective of the fabrication process, which may also govern the size-dependent mechanical behavior of the microspecimen. This diverse array of micro-manufacturing techniques is likely to keep expanding as novel methods continue to emerge from ongoing research and development efforts in this rapidly evolving field.

5. Conclusion

Focused ion beam milling, with its unique ability to carve test specimens specifically suited for the measurement of basic mechanical properties in essentially any material, has been one of the main driving forces, over the past two decades, behind advancements in the mechanical testing of small-scale material specimens. The method comes, as seen in the first part of this review, with a price, namely the fact that the microstructure of FIB-milled surfaces is often altered by ion and crystalline defect implantation. Progress has been achieved in recent years to reduce this effect, notably with the advent of inert-gas ion beams, yet the fact remains that ion-milled surfaces have undergone a high-energy material removal process that alters their microstructure and, at times, even their composition.

In parallel to the advent of FIB-milling as a means of producing micromechanical test samples, we have seen in the second part of this review that the range of available microscale materials processing methods has also witnessed significant advancements over the past two decades. This has in turn resulted in the advent of several viable alternatives to, or alterations of, traditional FIB-milling approaches for the production of high-quality, shaped micromechanical test samples, the surface microstructure of which has not been affected by ion-milling. Each of these techniques has its own advantages and disadvantages, and in certain scenarios and applications FIB-milling remains the most viable option at the moment, for example, when targeting particular microstructural features such as grain boundaries and complex compositions, or when dealing with radiation damage or oxide films. Yet, those alternative techniques are now well established, reproducible, and are growing in range. Some are even suitable for parallelized part production, such that, unlike FIB-milling, which is poorly fit for high-throughput production, their engineering importance is likely to grow.

The argument is therefore to be made that micromechanical test data from FIB-milled samples should be declared to be precisely that: data relevant to material that has been FIB-milled, nothing less - but also nothing more. Similarly, when samples are produced by nanomolding or microcasting, they will likely contain in their microstructure a signature of the process by which they were produced, namely a size-dependent density of dislocations that were formed to relieve thermal contraction mismatch strains; again, this will affect measured mechanical property data. We have to reckon that the processing method is an integral part of what defines a material when small-scale mechanical properties are reported – much as is the case when reporting macroscopic mechanical test data for brittle materials: reporting macroscopic strength measurements for, say, alumina has little meaning if one does not specify, with precision, how the test samples were produced. The same holds true for micro- or nano-mechanical test data. With this fact recognized, we further propose that it would be a worthwhile line of inquiry to substantially improve our understanding of what exactly is the influence of FIB-milling on the mechanical behavior of microscale samples, as a function of milling conditions and the nature of both the beam and the material. This is crucial not only because most work to date was produced using ion-milled microsamples, but also because for specific questions, such as the behavior of selected regions of a complex microstructure (say, a grain boundary), or the behavior at the microscale of materials for which no alternative exists to produce microsamples, this knowledge is required to separate fact from artifact.

In conclusion therefore, we motion that one must view the unique microstructural features introduced by different sample production methods as an integral part of what defines micromechanical material test data. Ultimately this will enrich our comprehension of materials and processing-microstructure-property relations in this intricate realm, but when studying materials at the micro- to nanoscale, will also lead to significant variation in what we still usually tend to view as a single, well-defined, “material”.

CRediT authorship contribution statement

Luciano Borasi: Writing – review & editing, Writing – original draft, Conceptualization. **Alejandra Slagter:** Writing – review & editing, Writing – original draft, Conceptualization. **Andreas Mortensen:** Writing – review & editing, Writing – original draft, Conceptualization. **Christoph Kirchlechner:** Writing – review & editing, Writing – original draft, Conceptualization.

Declaration of competing Interest

We, the authors of the article “*On the preparation and mechanical testing of nano- to micron-scale specimens*” declare that we do not have competing financial interests or personal relationships that could have appeared to influence the work reported in this article.

Acknowledgements

This work was performed with partial sponsorship from base laboratory budgets of the Laboratory for Mechanical Metallurgy (LMM) at the Ecole Polytechnique Fédérale de Lausanne (EPFL), and of the Institute for Applied Materials – Mechanics of Materials and Interfaces (IAM-MMI) at the Karlsruhe Institute of Technology. LB and AS acknowledge

the support of the SNSF through Postdoc.Mobility fellowships P500PN_217723 and P500PN_217937, respectively. The authors would like to thank the following colleagues for illuminating discussion of the subject of this review (but remain solely responsible for its contents): Dr. Marc Legros of the CEMES-CNRS in Toulouse, France, and Prof. Helena van Swygenhoven of the Paul Scherrer Institute in Villingen, Switzerland.

References

[1] M.D. Uchic, D.M. Dimiduk, J.N. Florando, W.D. Nix, Exploring specimen size effects in plastic deformation of Ni3(Al, Ta), MRS Online Proc. Lib. 753 (2003) 14, https://doi.org/10.1557/PROC-753-BB1.4.
[2] M.D. Uchic, Sample dimensions influence strength and crystal plasticity, Science (1979) 305 (2004) 986–989, https://doi.org/10.1126/science.1098993.
[3] K.J. Hemker, W.N. Sharpe, Microscale characterization of mechanical properties, Annu. Rev. Mater. Res. 37 (2007) 93–126, https://doi.org/10.1146/annurev.matsci.36.062705.134551.
[4] Y. Zhu, C. Ke, H.D. Espinosa, Experimental techniques for the mechanical characterization of one-dimensional nanostructures, Exp. Mech. 47 (2007) 7–24, https://doi.org/10.1007/s11340-006-0406-6.
[5] M.D. Uchic, P.A. Shade, D.M. Dimiduk, Plasticity of micrometer-scale single crystals in compression, Ann. Rev. Mater. Res. 39 (2009) 361–386, https://doi.org/10.1146/annurev-matsci-082908-145422.
[6] D.S. Gianola, C. Eberl, Micro- and nanoscale tensile testing of materials, JOM 61 (2009) 24–35, https://doi.org/10.1007/s11837-009-0037-3.
[7] O. Kraft, P.A. Gruber, R. Mönig, D. Weygand, Plasticity in confined dimensions, Annu. Rev. Mater. Res. 40 (2010) 293–317, https://doi.org/10.1146/annurev-matsci-082908-145409.
[8] M. Legros, D.S. Gianola, C. Motz, Quantitative in situ mechanical testing in electron microscopes, MRS Bull. 35 (2010) 354–360, https://doi.org/10.1557/mrs2010.567.
[9] J.R. Greer, J.Th.M. De Hosson, Plasticity in small-sized metallic systems: intrinsic versus extrinsic size effect, Prog. Mater. Sci. 56 (2011) 654–724, https://doi.org/10.1016/j.pmatsci.2011.01.005.
[10] M. Legros, Small Scale Plasticity - A Review. Mechanics of Nano-Objects, Samuel Forest, Anne Ponchet and Olivier Thomas Editors, Transvalor - Presse Des Mines, 2011, pp. 241–267.
[11] M.F. Pantano, H.D. Espinosa, L. Pagnotta, Mechanical characterization of materials at small length scales, J. Mech. Sci. Technol. 26 (2012) 545–561, https://doi.org/10.1007/s12206-011-1214-1.
[12] Q. Yu, M. Legros, A.M. Minor, situ TEM nanomechanics, MRS Bull. 40 (2015) 62–70, https://doi.org/10.1557/mrs.2014.306.
[13] W. Kang, M. Merrill, J.M. Wheeler, In situ thermomechanical testing methods for micro/nano-scale materials, Nanoscale 9 (2017) 2666–2688, https://doi.org/10.1039/C6NR07330A.
[14] R. Maaß, P.M. Derlet, Micro-plasticity and recent insights from intermittent and small-scale plasticity, Acta Mater. 143 (2018) 338–363, https://doi.org/10.1016/j.actamat.2017.06.023.
[15] G. Dehm, B.N. Jaya, R. Raghavan, C. Kirchlechner, Overview on micro- and nanomechanical testing: new insights in interface plasticity and fracture at small length scales, Acta Mater. 142 (2018) 248–282, https://doi.org/10.1016/j.actamat.2017.06.019.
[16] R. Pippan, S. Wurster, D. Kiener, Fracture mechanics of micro samples: fundamental considerations, Mater. Des. 159 (2018) 252–267, https://doi.org/10.1016/j.matdes.2018.09.004.
[17] J. Ast, M. Ghidelli, K. Durst, M. Göken, M. Sebastiani, A.M. Korsunsky, A review of experimental approaches to fracture toughness evaluation at the micro-scale, Mater. Des. 173 (2019) 107762, https://doi.org/10.1016/j.matdes.2019.107762.
[18] A.M. Minor, G. Dehm, Advances in in situ nanomechanical testing, MRS Bull. 44 (2019) 438–442, https://doi.org/10.1557/mrs.2019.127.
[19] V. Jayaram, Small-scale mechanical testing, Annu. Rev. Mater. Res. 52 (2022) 473–523, https://doi.org/10.1146/annurev-matsci-080819-123640.
[20] B.N. Jaya, N.G. Mathews, A.K. Mishra, S. Basu, K. Jacob, Non-conventional small-scale mechanical testing of materials, J. Indian Inst. Sci. 102 (2022) 139–171, https://doi.org/10.1007/s41745-022-00302-3.
[21] D. Kiener, M. Wurmshuber, M. Alfreider, G.J.K. Schaffar, V. Maier-Kiener, Recent advances in nanomechanical and in situ testing techniques: towards extreme conditions, Curr. Opin. Solid State Mater. Sci. 27 (2023) 101108, https://doi.org/10.1016/j.cossms.2023.101108.
[22] D. Kiener, A. Misra, Nanomechanical characterization, MRS Bull. (2023), https://doi.org/10.1557/s43577-023-00643-z.
[23] M.D. Uchic, D.M. Dimiduk, A methodology to investigate size scale effects in crystalline plasticity using uniaxial compression testing, Mater. Sci. Eng.: A 400–401 (2005) 268–278, https://doi.org/10.1016/j.msea.2005.03.082.
[24] M.G. Mueller, G. Žagar, A. Mortensen, Stable room-temperature micron-scale crack growth in single-crystalline silicon, J. Mater. Res. 32 (2017) 3617–3626, https://doi.org/10.1557/jmr.2017.238.
[25] Z. Fu, L. Jiang, J.L. Wardini, B.E. MacDonald, H. Wen, W. Xiong, D. Zhang, Y. Zhou, T.J. Rupert, W. Chen, E.J. Lavernia, A high-entropy alloy with hierarchical nanoprecipitates and ultrahigh strength, Sci. Adv. 4 (2018) eaat8712, https://doi.org/10.1126/sciadv.aat8712.
[26] R. Hosseinabadi, A. Brognara, C. Kirchlechner, J.P. Best, G. Dehm, The role of incoherent twin boundaries on the plasticity of Cu micropillars, Mater. Des. 232 (2023) 112164, https://doi.org/10.1016/j.matdes.2023.112164.
[27] S. Reyntjens, R. Puers, A review of focused ion beam applications in microsystem technology, J. Micromech. Microeng. 11 (2001) 287–300, https://doi.org/10.1088/0960-1317/11/4/301.
[28] C.A. Volkert, A.M. Minor, Focused ion beam microscopy and micromachining, MRS Bull. 32 (2007) 389–399, https://doi.org/10.1557/mrs2007.62.
[29] K. Gamo, S. Namba, Microfabrication using focused ion beams, Euro III-Vs Rev. 3 (1990) 41–42, https://doi.org/10.1016/0959-3527(90)90205-8.
[30] R.M. Langford, P.M. Nellen, J. Gierak, Y. Fu, Focused Ion Beam Micro- and Nanoengineering, MRS Bull 32 (2007) 417–423, https://doi.org/10.1557/mrs2007.65.
[31] J. Orloff, L. Swanson, M. Utlaut, High Resolution Focused Ion Beams: FIB and Its Applications: Fib and Its Applications : The Physics of Liquid Metal Ion Sources and Ion Optics and Their Application to Focused Ion Beam Technology, Springer Science & Business Media, 2003.
[32] E.I. Preiß, B. Merle, Y. Xiao, F. Gannott, J.P. Liebig, J.M. Wheeler, M. Göken, Applicability of focused Ion beam (FIB) milling with gallium, neon, and xenon to the fracture toughness characterization of gold thin films, J. Mater. Res. 36 (2021) 2505–2514, https://doi.org/10.1557/s43578-020-00045-w.
[33] S.A. Boden, Z. Moktadir, D.M. Bagnall, H. Mizuta, H.N. Rutt, Focused helium ion beam milling and deposition, Microelectron. Eng. 88 (2011) 2452–2455, https://doi.org/10.1016/j.mee.2010.11.041.
[34] M. Nastasi, J.W. Mayer, J.K. Hirvonen, Ion-Solid Interactions: Fundamentals and Applications, Cambridge University Press, 1996.
[35] R. Schwaiger, M. Weber, B. Moser, P. Gumbsch, O. Kraft, Mechanical assessment of ultrafine-grained nickel by microcompression experiment and finite element simulation, J. Mater. Res. 27 (2012) 266–277, https://doi.org/10.1557/jmr.2011.248.
[36] D. Raabe, D. Ma, F. Roters, Effects of initial orientation, sample geometry and friction on anisotropy and crystallographic orientation changes in single crystal microcompression deformation: a crystal plasticity finite element study, Acta Mater. 55 (2007) 4567–4583, https://doi.org/10.1016/j.actamat.2007.04.023.
[37] D.M. Dimiduk, M.D. Uchic, T.A. Parthasarathy, Size-affected single-slip behavior of pure nickel microcrystals, Acta Mater. 53 (2005) 4065–4077, https://doi.org/10.1016/j.actamat.2005.05.023.
[38] A. Ernst, M. Wei, M. Aindow, A comparison of Ga FIB and Xe-Plasma FIB of complex Al alloys, Microsc. Microanal. 23 (2017) 288–289, https://doi.org/10.1017/S1431927617002124.
[39] B. Tordoff, C. Hartfield, A.J. Holwell, S. Hiller, M. Kaestner, S. Kelly, J. Lee, S. Müller, F. Perez-Willard, T. Volkenandt, R. White, T. Rodgers, The LaserFIB: new application opportunities combining a high-performance FIB-SEM with femtosecond laser processing in an integrated second chamber, Appl. Microsc. 50 (2020) 24, https://doi.org/10.1186/s42649-020-00044-5.
[40] M.P. Echlin, A.T. Polonsky, J. Lamb, R. Geurts, S.J. Randolph, A. Botman, T. M. Pollock, Recent developments in femtosecond laser-enabled TriBeam systems, JOM 73 (2021) 4258–4269, https://doi.org/10.1007/s11837-021-04919-0.
[41] M.P. Echlin, M. Straw, S. Randolph, J. Filevich, T.M. Pollock, The TriBeam system: femtosecond laser ablation in situ SEM, Mater. Charact. 100 (2015) 1–12, https://doi.org/10.1016/j.matchar.2014.10.023.
[42] S.Y. Kim, S. Kavak, K.G. Bayrak, C. Sun, H. Xu, M.J. Lee, D. Chen, Y. Zhang, E. Tekoğlu, D. Ağaoğulları, E. Ayas, E.S. Park, J. Li, Demonstration of Helide formation for fusion structural materials as natural lattice sinks for helium, Acta Mater. 266 (2024) 119654, https://doi.org/10.1016/j.actamat.2024.119654.
[43] J.D. Casey Jr., M. Phaneuf, C. Chandler, M. Megorden, K.E. Noll, R. Schuman, T. J. Gannon, A. Krechmer, D. Monforte, N. Antoniou, N. Bassom, J. Li, P. Carleson, C. Huynh, Copper device editing: strategy for focused ion beam milling of copper, J. Vacuum Sci. Technol. B: Microelectron. Nanometer Struct. Process. Measur. Phenomena 20 (2002) 2682–2685, https://doi.org/10.1116/1.1521736.
[44] M.W. Phaneuf, J. Li, J.D. Casey, Gallium phase formation in Cu and Other FCC metals during near-normal incidence Ga-FIB milling and techniques to avoid this phenomenon, Microsc. Microanal. 8 (2002) 52–53, https://doi.org/10.1017/S1431927602101589.
[45] S.M. Hanlon, S.Y. Persaud, F. Long, A. Korinek, M.R. Daymond, A solution to FIB induced artefact hydrides in Zr alloys, J. Nucl. Mater. 515 (2019) 122–134, https://doi.org/10.1016/j.jnucmat.2018.12.020.
[46] S. Abolhassani, P. Gasser, Preparation of TEM samples of metal–oxide interface by the focused ion beam technique, J. Microsc. 223 (2006) 73–82, https://doi.org/10.1111/j.1365-2818.2006.01599.x.
[47] S.K. Marya, G. Wyon, Temporary embrittlement followed by increase in ductility after gallium penetration in cold rolled aluminium, Scripta Metallurgica 9 (1975) 1009–1016, https://doi.org/10.1016/0036-9748(75)90270-7.
[48] E. Pereiro-López, W. Ludwig, D. Bellet, P. Cloetens, C. Lemaignan, Direct evidence of Nanometric Invasionlike grain boundary penetration in the $ \mathrm{Al}/\mathrm{Ga}$ system, Phys. Rev. Lett. 95 (2005) 215501, https://doi.org/10.1103/PhysRevLett.95.215501.
[49] E. Pereiro-López, W. Ludwig, D. Bellet, C. Lemaignan, In situ investigation of Al bicrystal embrittlement by liquid Ga using synchrotron imaging, Acta Mater. 54 (2006) 4307–4316, https://doi.org/10.1016/j.actamat.2006.05.021.
[50] K.a. Unocic, M.j. Mills, G.s. Daehn, Effect of gallium focused ion beam milling on preparation of aluminium thin foils, J. Microsc. 240 (2010) 227–238, https://doi.org/10.1111/j.1365-2818.2010.03401.x.
[51] H.-S. Nam, D.J. Srolovitz, Effect of material properties on liquid metal embrittlement in the Al–Ga system, Acta Mater. 57 (2009) 1546–1553, https://doi.org/10.1016/j.actamat.2008.11.041.

[52] C.L. Briant, Embrittlement of Engineering Alloys, Elsevier, 2013.
[53] K. Eder, V. Bhatia, J. Qu, B. Van Leer, M. Dutka, J.M. Cairney, A multi-ion plasma FIB study: determining ion implantation depths of Xe, N, O and Ar in tungsten via atom probe tomography, Ultramicroscopy. 228 (2021) 113334, https://doi.org/10.1016/j.ultramic.2021.113334.
[54] X. Zhong, C.A. Wade, P.J. Withers, X. Zhou, C. Cai, S.J. Haigh, M.G. Burke, Comparing Xe+pFIB and Ga+FIB for TEM sample preparation of Al alloys: minimising FIB-induced artefacts, J. Microsc. 282 (2021) 101–112, https://doi.org/10.1111/jmi.12983.
[55] G.S. Was, Ion beam modification of metals: compositional and microstructural changes, Prog. Surf. Sci. 32 (1989) 211–332, https://doi.org/10.1016/0079-6816(89)90005-1.
[56] L.A. Giannuzzi, F.A. Stevie, A review of focused ion beam milling techniques for TEM specimen preparation, Micron. 30 (1999) 197–204, https://doi.org/10.1016/S0968-4328(99)00005-0.
[57] J. Mayer, L.A. Giannuzzi, T. Kamino, J. Michael, TEM sample preparation and FIB-induced damage, MRS Bull. 32 (2007) 400–407, https://doi.org/10.1557/mrs2007.63.
[58] E. Salvati, L.R. Brandt, C. Papadaki, H. Zhang, S.M. Mousavi, D. Wermeille, A. M. Korsunsky, Nanoscale structural damage due to focused ion beam milling of silicon with Ga ions, Mater. Lett. 213 (2018) 346–349, https://doi.org/10.1016/j.matlet.2017.11.043.
[59] M. Tamura, S. Shukuri, M. Moniwa, M. Default, Focused ion beam gallium implantation into silicon, Appl. Phys. A 39 (1986) 183–190, https://doi.org/10.1007/BF00620733.
[60] T.L. Burnett, R. Kelley, B. Winiarski, L. Contreras, M. Daly, A. Gholinia, M. G. Burke, P.J. Withers, Large volume serial section tomography by Xe Plasma FIB dual beam microscopy, Ultramicroscopy. 161 (2016) 119–129, https://doi.org/10.1016/j.ultramic.2015.11.001.
[61] K.E. Knipling, D.J. Rowenhorst, R.W. Fonda, G. Spanos, Effects of focused ion beam milling on austenite stability in ferrous alloys, Mater. Charact. 61 (2010) 1–6, https://doi.org/10.1016/j.matchar.2009.09.013.
[62] H.G. Jones, A.P. Day, D.C. Cox, Electron backscatter diffraction studies of focused ion beam induced phase transformation in cobalt, Mater. Charact. 120 (2016) 210–219, https://doi.org/10.1016/j.matchar.2016.09.004.
[63] E.H. Lee, Ion-beam modification of polymeric materials – fundamental principles and applications, Nucl. Instrument. Method. Phys. Res. Sect. B: Beam Interact. Mater. Atoms 151 (1999) 29–41, https://doi.org/10.1016/S0168-583X(99)00129-9.
[64] N.d. Bassim, B.t. De Gregorio, A.l.d. Kilcoyne, K. Scott, T. Chou, S. Wirick, G. Cody, R. m. Stroud, Minimizing damage during FIB sample preparation of soft materials, J. Microsc. 245 (2012) 288–301, https://doi.org/10.1111/j.1365-2818.2011.03570.x.
[65] M. Sezen, H. Plank, E. Fisslthaler, B. Chernev, A. Zankel, E. Tchernychova, A. Blümel, E.J.W. List, W. Grogger, P. Pölt, An investigation on focused electron/ion beam induced degradation mechanisms of conjugated polymers, Phys. Chem. Chem. Phys. 13 (2011) 20235–20240, https://doi.org/10.1039/C1CP22406A.
[66] S. Lee, J. Jeong, Y. Kim, S.M. Han, D. Kiener, S.H. Oh, FIB-induced dislocations in Al submicron pillars: annihilation by thermal annealing and effects on deformation behavior, Acta Mater. 110 (2016) 283–294, https://doi.org/10.1016/j.actamat.2016.03.017.
[67] D. Kiener, C. Motz, M. Rester, M. Jenko, G. Dehm, FIB damage of Cu and possible consequences for miniaturized mechanical tests, Mater. Sci. Eng.: A 459 (2007) 262–272, https://doi.org/10.1016/j.msea.2007.01.046.
[68] F. Hofmann, E. Tarleton, R.J. Harder, N.W. Phillips, P.-W. Ma, J.N. Clark, I. K. Robinson, B. Abbey, W. Liu, C.E. Beck, 3D lattice distortions and defect structures in ion-implanted nano-crystals, Sci. Rep. 7 (2017) 45993, https://doi.org/10.1038/srep45993.
[69] C.A. B, S.M. A, B.V. I, P.D. E, M.L. A, L.M. E, Development of the surface morphology of germanium upon irradiation with gallium ions, St. Petersburg Polytechnic Univ. J.: Phys. Math. 68 (2023) 21–25, https://doi.org/10.18721/JPM.163.103.
[70] D. Xia, Y.-B. Jiang, J. Notte, D. Runt, GaAs milling with neon focused ion beam: comparison with gallium focused ion beam milling and subsurface damage analysis, Appl. Surf. Sci. 538 (2021) 147922. https://doi.org/10.1016/j.apsusc.2020.147922.</bib.
[71] R. Maaβ, D. Grolimund, S. Van Petegem, M. Willimann, M. Jensen, H. Van Swygenhoven, T. Lehnert, M.A.M. Gijs, C.A. Volkert, E.T. Lilleodden, R. Schwaiger, Defect structure in micropillars using x-ray microdiffraction, Appl. Phys. Lett. 89 (2006) 151905, https://doi.org/10.1063/1.2358204.
[72] R. Maaß, S. Van Petegem, H. Van Swygenhoven, P.M. Derlet, C.A. Volkert, D. Grolimund, Time-resolved laue diffraction of deforming micropillars, Phys. Rev. Lett. 99 (2007) 145505, https://doi.org/10.1103/PhysRevLett.99.145505.
[73] R. Maaß, S. Van Petegem, J. Zimmermann, C.N. Borca, H. Van Swygenhoven, On the initial microstructure of metallic micropillars, Scr. Mater. 59 (2008) 471–474, https://doi.org/10.1016/j.scriptamat.2008.04.034.
[74] Z.-J. Wang, F.I. Allen, Z.-W. Shan, P. Hosemann, Mechanical behavior of copper containing a gas-bubble superlattice, Acta Mater. 121 (2016) 78–84, https://doi.org/10.1016/j.actamat.2016.08.085.
[75] W.-Z. Han, J. Zhang, M.-S. Ding, L. Lv, W.-H. Wang, G.-H. Wu, Z.-W. Shan, J. Li, Helium nanobubbles enhance superelasticity and retard shear localization in small-volume shape memory alloy, Nano Lett. 17 (2017) 3725–3730, https://doi.org/10.1021/acs.nanolett.7b01015.
[76] M.-S. Ding, J.-P. Du, L. Wan, S. Ogata, L. Tian, E. Ma, W.-Z. Han, J. Li, Z.-W. Shan, Radiation-Induced helium nanobubbles enhance ductility in submicron-sized single-crystalline copper, Nano Lett. 16 (2016) 4118–4124, https://doi.org/10.1021/acs.nanolett.6b00864.
[77] On the use of SRIM for computing radiation damage exposure, Nucl. Instrument. Method. Phys. Res. Sect. B: Beam Interact. Mater. Atoms 310 (2013) 75–80, https://doi.org/10.1016/j.nimb.2013.05.008.
[78] A. Lotnyk, D. Poppitz, U. Ross, J.W. Gerlach, F. Frost, S. Bernütz, E. Thelander, B. Rauschenbach, Focused high- and low-energy ion milling for TEM specimen preparation, Microelectron. Reliab. 55 (2015) 2119–2125, https://doi.org/10.1016/j.microrel.2015.07.005.
[79] A.D. Norton, S. Falco, N. Young, J. Severs, R.I. Todd, Microcantilever investigation of fracture toughness and subcritical crack growth on the scale of the microstructure in Al2O3, J. Eur. Ceram. Soc. 35 (2015) 4521–4533, https://doi.org/10.1016/j.jeurceramsoc.2015.08.023.
[80] J. Hütsch, E.T. Lilleodden, The influence of focused-ion beam preparation technique on microcompression investigations: lathe vs. annular milling, Scr. Mater. 77 (2014) 49–51, https://doi.org/10.1016/j.scriptamat.2014.01.016.
[81] K. Pandey, K. Paredis, T. Hantschel, C. Drijbooms, W. Vandervorst, The impact of focused ion beam induced damage on scanning spreading resistance microscopy measurements, Sci. Rep. 10 (2020) 1–15, https://doi.org/10.1038/s41598-020-71826-w.
[82] M. Presley, J. Jensen, D. Huber, H. Fraser, Exploring differences in amorphous layer formation during FIB sample preparation between metals and non metals, Microsc. Microanal. 22 (2016) 144–145, https://doi.org/10.1017/S1431927616001574.
[83] S. Rubanov, P.R. Munroe, FIB-induced damage in silicon, J. Microsc. 214 (2004) 213–221, https://doi.org/10.1111/j.0022-2720.2004.01327.x.
[84] T.L. Matteson, S.W. Schwarz, E.C. Houge, B.W. Kempshall, L.A. Giannuzzi, Electron backscattering diffraction investigation of focused ion beam surfaces, J. Electron. Mater. 31 (2002) 33–39, https://doi.org/10.1007/s11664-002-0169-5.
[85] C. Kirchlechner, Dislocation slip transfer mechanisms: quantitative insights from in situ micromechanical testing, Habilitation thesis, 2017.
[86] C. Kirchlechner, P.J. Imrich, W. Grosinger, M.W. Kapp, J. Keckes, J.S. Micha, O. Ulrich, O. Thomas, S. Labat, C. Motz, G. Dehm, Expected and unexpected plastic behavior at the micron scale: an in situ μLaue tensile study, Acta Mater. 60 (2012) 1252–1258, https://doi.org/10.1016/j.actamat.2011.10.058.
[87] R. Gu, A.H.W. Ngan, Effects of pre-straining and coating on plastic deformation of aluminum micropillars, Acta Mater. 60 (2012) 6102–6111, https://doi.org/10.1016/j.actamat.2012.07.048.
[88] D. Kiener, Z. Zhang, S. Šturm, S. Cazottes, P.J. Imrich, C. Kirchlechner, G. Dehm, Advanced nanomechanics in the TEM: effects of thermal annealing on FIB prepared Cu samples, Philos. Mag. 92 (2012) 3269–3289, https://doi.org/10.1080/14786435.2012.685966.
[89] T. Vermeij, E. Plancher, C.C. Tasan, Preventing damage and redeposition during focused ion beam milling: the “umbrella” method, Ultramicroscopy. 186 (2018) 35–41, https://doi.org/10.1016/j.ultramic.2017.12.012.
[90] G. Bailey, S. McKernan, R. Price, S. Walck, P.-M. Charest, R. Gauvin, R. B. Jamison, A.J. Mardinly, D.W. Susnitzky, R. Gronsky, Effects of ion species and energy on the Amorphization of Si during FIB TEM sample preparation as determined by computational and experimental methods, Microsc. Microanal. 6 (2000) 526–527, https://doi.org/10.1017/S1431927600035121.
[91] S. Bals, W. Tirry, R. Geurts, Z. Yang, D. Schryvers, High-quality sample preparation by low kV FIB thinning for analytical TEM measurements, Microsc. Microanal. 13 (2007) 80–86, https://doi.org/10.1017/S1431927607070018.
[92] Y. Yang, S.Y. Wang, B. Xiang, S. Yin, T.C. Pekin, X. Li, R. Zhang, K. Yano, D. Hwang, M. Asta, C. Grigoropoulos, F.I. Allen, A.M. Minor, Evaluating the effects of pillar shape and gallium ion beam damage on the mechanical properties of single crystal aluminum nanopillars, J. Mater. Res. 36 (2021) 2515–2528, https://doi.org/10.1557/s43578-021-00125-5.
[93] L. Giannuzzi, N. Smith, TEM specimen preparation with plasma FIB Xe+ ions, Microsc. Microanal. 17 (2011) 646–647, https://doi.org/10.1017/S1431927611004107.
[94] P.D. Edmondson, K.J. Abrams, J.A. Hinks, G. Greaves, C.J. Pawley, I. Hanif, S. E. Donnelly, An in situ transmission electron microscopy study of the ion irradiation induced amorphisation of silicon by He and Xe, Scr. Mater. 113 (2016) 190–193, https://doi.org/10.1016/j.scriptamat.2015.11.010.
[95] S.T. Murphy, P. Fossati, R.W. Grimes, Xe diffusion and bubble nucleation around edge dislocations in UO2, J. Nucl. Mater. 466 (2015) 634–637, https://doi.org/10.1016/j.jnucmat.2015.09.007.
[96] J.P. Liebig, M. Göken, G. Richter, M. Mačković, T. Przybilla, E. Spiecker, O. N. Pierron, B. Merle, A flexible method for the preparation of thin film samples for in situ TEM characterization combining shadow-FIB milling and electron-beam-assisted etching, Ultramicroscopy. 171 (2016) 82–88, https://doi.org/10.1016/j.ultramic.2016.09.004.
[97] M.B. Lowry, D. Kiener, M.M. LeBlanc, C. Chisholm, J.N. Florando, J.W. Morris, A. M. Minor, Achieving the ideal strength in annealed molybdenum nanopillars, Acta Mater. 58 (2010) 5160–5167, https://doi.org/10.1016/j.actamat.2010.05.052.
[98] J. Jeong, S. Lee, Y. Kim, S.M. Han, D. Kiener, Y.-B. Kang, S.H. Oh, Microstructural evolution of a focused ion beam fabricated Mg nanopillar at high temperatures: defect annihilation and sublimation, Scr. Mater. 86 (2014) 44–47, https://doi.org/10.1016/j.scriptamat.2014.05.009.
[99] J.R. Greer, W.D. Nix, Nanoscale gold pillars strengthened through dislocation starvation, Phys. Rev. B 73 (2006) 245410, https://doi.org/10.1103/PhysRevB.73.245410.

[100] A.T. Jennings, J.R. Greer, Tensile deformation of electroplated copper nanopillars, Philos. Mag. 91 (2011) 1108–1120, https://doi.org/10.1080/14786435.2010.505180.
[101] S. Shim, H. Bei, M.K. Miller, G.M. Pharr, E.P. George, Effects of focused ion beam milling on the compressive behavior of directionally solidified micropillars and the nanoindentation response of an electropolished surface, Acta Mater. 57 (2009) 503–510, https://doi.org/10.1016/j.actamat.2008.09.033.
[102] M. Dietiker, S. Buzzi, G. Pigozzi, J.F. Löffler, R. Spolenak, Deformation behavior of gold nano-pillars prepared by nanoimprinting and focused ion-beam milling, Acta Mater. 59 (2011) 2180–2192, https://doi.org/10.1016/j.actamat.2010.12.019.
[103] C. Griesbach, S.-J. Jeon, D.F. Rojas, M. Ponga, S. Yazdi, S. Pathak, N. Mara, E. L. Thomas, R. Thevamaran, Origins of size effects in initially dislocation-free single-crystal silver micro- and nanocubes, Acta Mater. (2021) 117020, https://doi.org/10.1016/j.actamat.2021.117020.
[104] J. Krebs, S.I. Rao, S. Verheyden, C. Miko, R. Goodall, W.A. Curtin, A. Mortensen, Cast aluminium single crystals cross the threshold from bulk to size-dependent stochastic plasticity, Nature Mater 16 (2017) 730–736, https://doi.org/10.1038/nmat4911.
[105] L. Borasi, S. Frasca, E. Charbon, A. Mortensen, The effect of size, orientation and temperature on the deformation of microcast silver crystals, Acta Mater. (2023) 118817, https://doi.org/10.1016/j.actamat.2023.118817.
[106] C. Motz, T. Schöberl, R. Pippan, Mechanical properties of micro-sized copper bending beams machined by the focused ion beam technique, Acta Mater. 53 (2005) 4269–4279, https://doi.org/10.1016/j.actamat.2005.05.036.
[107] D. Kiener, C. Motz, T. Schöberl, M. Jenko, G. Dehm, Determination of mechanical properties of copper at the micron scale, Adv. Eng. Mater. 8 (2006) 1119–1125, https://doi.org/10.1002/adem.200600129.
[108] L. Kubin, Dislocations, Mesoscale Simulations and Plastic Flow, 1st edition, Oxford University Press, Oxford, United Kingdom, 2013.
[109] R.L. Fleisgher, Solution hardening, Acta Metallurgica 9 (1961) 996–1000, https://doi.org/10.1016/0001-6160(61)90242-5.
[110] M.Z. Butt, P. Feltham, Solid-solution hardening, J. Mater. Sci. 28 (1993) 2557–2576, https://doi.org/10.1007/BF00356192.
[111] F.R.N. Nabarro, The theory of solution hardening, Philos. Mag.: a J. Theor. Exp. Appl. Phys. 35 (1977) 613–622, https://doi.org/10.1080/14786437708235994.
[112] R. Labusch, A statistical theory of solid solution hardening, Physica Status Solidi (b) 41 (1970) 659–669, https://doi.org/10.1002/pssb.19700410221.
[113] J.A. El-Awady, C. Woodward, D.M. Dimiduk, N.M. Ghoniem, Effects of focused ion beam induced damage on the plasticity of micropillars, Phys. Rev. B 80 (2009) 104104, https://doi.org/10.1103/PhysRevB.80.104104.
[114] E. Hornbogen, Hundred years of precipitation hardening, J. Light Metals 1 (2001) 127–132, https://doi.org/10.1016/S1471-5317(01)00006-2.
[115] D.J. Magagnosc, R. Ehrbar, G. Kumar, M.R. He, J. Schroers, D.S. Gianola, Tunable tensile ductility in metallic glasses, Sci. Rep. 3 (2013) 1096, https://doi.org/10.1038/srep01096.
[116] D.J. Magagnosc, G. Kumar, J. Schroers, P. Felfer, J.M. Cairney, D.S. Gianola, Effect of ion irradiation on tensile ductility, strength and fictive temperature in metallic glass nanowires, Acta Mater. 74 (2014) 165–182, https://doi.org/10.1016/j.actamat.2014.04.002.
[117] H. Bei, S. Shim, M.K. Miller, G.M. Pharr, E.P. George, Effects of focused ion beam milling on the nanomechanical behavior of a molybdenum-alloy single crystal, Appl. Phys. Lett. 91 (2007) 111915, https://doi.org/10.1063/1.2784948.
[118] J.R. Greer, H. Espinosa, K.T. Ramesh, E. Nadgorny, Comment on “Effects of focused ion beam milling on the nanomechanical behavior of a molybdenum-alloy single crystal, Appl. Phys. Lett. 91, 111915 (2007), Appl. Phys. Lett. 92 (2008) 096101, https://doi.org/10.1063/1.2889997.
[119] K.E. Johanns, A. Sedlmayr, P.S. Phani, R. Mönig, O. Kraft, E.P. George, G. M. Pharr, In-situ tensile testing of single-crystal molybdenum-alloy fibers with various dislocation densities in a scanning electron microscope, J. Mater. Res. 27 (2012) 508–520, https://doi.org/10.1557/jmr.2011.298.
[120] H. Bei, S. Shim, E. George, M. Miller, E. Herbert, G. Pharr, Compressive strengths of molybdenum alloy micro-pillars prepared using a new technique, Scr. Mater. 57 (2007) 397–400, https://doi.org/10.1016/j.scriptamat.2007.05.010.
[121] H. Bei, S. Shim, G.M. Pharr, E.P. George, Effects of pre-strain on the compressive stress–strain response of Mo-alloy single-crystal micropillars, Acta Mater. 56 (2008) 4762–4770, https://doi.org/10.1016/j.actamat.2008.05.030.
[122] R. Maaß, L. Meza, B. Gan, S. Tin, Julia.R. Greer, Ultrahigh strength of dislocation-free Ni3Al nanocubes, Small. 8 (2012) 1869–1875, https://doi.org/10.1002/smll.201102603.
[123] S.-W. Lee, D. Mordehai, E. Rabkin, W.D. Nix, Effects of focused-ion-beam irradiation and prestraining on the mechanical properties of FCC Au microparticles on a sapphire substrate, J. Mater. Res. 26 (2011) 1653–1661, https://doi.org/10.1557/jmr.2011.221.
[124] M. Sedore, B.J. Diak, A. Murray, B. Riel, Comparison of the elastic-plastic transition in nanocrystalline nickel pillars fabricated by electron beam lithography and focused ion beam methods, IOP Conf. Ser.: Mater. Sci. Eng. 580 (2019) 012023, https://doi.org/10.1088/1757-899X/580/1/012023.
[125] Y. Xiao, J. Wehrs, H. Ma, T. Al-Samman, S. Korte-Kerzel, M. Göken, J. Michler, R. Spolenak, J.M. Wheeler, Investigation of the deformation behavior of aluminum micropillars produced by focused ion beam machining using Ga and Xe ions, Scr. Mater. 127 (2017) 191–194, https://doi.org/10.1016/j.scriptamat.2016.08.028.
[126] Y. Xiao, V. Maier-Kiener, J. Michler, R. Spolenak, J.M. Wheeler, Deformation behavior of aluminum pillars produced by Xe and Ga focused ion beams: insights from strain rate jump tests, Mater. Des. 181 (2019) 107914, https://doi.org/10.1016/j.matdes.2019.107914.
[127] J. Liu, R. Niu, J. Gu, M. Cabral, M. Song, X. Liao, Effect of ion irradiation introduced by focused ion-beam milling on the mechanical behaviour of sub-micron-sized samples, Sci. Rep. 10 (2020) 10324, https://doi.org/10.1038/s41598-020-66564-y.
[128] D. Kiener, W. Grosinger, G. Dehm, R. Pippan, A further step towards an understanding of size-dependent crystal plasticity: in situ tension experiments of miniaturized single-crystal copper samples, Acta Mater. 56 (2008) 580–592, https://doi.org/10.1016/j.actamat.2007.10.015.
[129] L. Borasi, S. Frasca, K. Nicolet-Dit-Felix, E. Charbon, A. Mortensen, Coupling silicon lithography with metal casting, Appl. Mater. Today 29 (2022) 101647, https://doi.org/10.1016/j.apmt.2022.101647.
[130] B.N. Jaya, V. Jayaram, Fracture testing at small-length scales: from plasticity in Si to brittleness in Pt, JOM 68 (2016) 94–108, https://doi.org/10.1007/s11837-015-1489-2.
[131] F.W. DelRio, R.F. Cook, B.L. Boyce, Fracture strength of micro- and nano-scale silicon components, Appl. Phys. Rev. 2 (2015) 021303, https://doi.org/10.1063/1.4919540.
[132] B.N. Jaya, C. Kirchlechner, G. Dehm, Can microscale fracture tests provide reliable fracture toughness values? A case study in silicon, J. Mater. Res. 30 (2015) 686–698, https://doi.org/10.1557/jmr.2015.2.
[133] J.P. Best, J. Zechner, I. Shorubalko, J.V. Oboňa, J. Wehrs, M. Morstein, J. Michler, A comparison of three different notching ions for small-scale fracture toughness measurement, Scr. Mater. 112 (2016) 71–74, https://doi.org/10.1016/j.scriptamat.2015.09.014.
[134] N.R. Velez, F.I. Allen, M.A. Jones, J. Donohue, W. Li, K. Pister, S. Govindjee, G. F. Meyers, A.M. Minor, Nanomechanical testing of freestanding polymer films: in situ tensile testing and Tg measurement, J. Mater. Res. 36 (2021) 2456–2464, https://doi.org/10.1557/s43578-021-00163-z.
[135] K. Zheng, C. Wang, Y.-Q. Cheng, Y. Yue, X. Han, Z. Zhang, Z. Shan, S.X. Mao, M. Ye, Y. Yin, E. Ma, Electron-beam-assisted superplastic shaping of nanoscale amorphous silica, Nat. Commun. 1 (2010) 24, https://doi.org/10.1038/ncomms1021.
[136] S. Bruns, C. Minnert, L. Pethö, J. Michler, K. Durst, Room temperature viscous flow of amorphous silica induced by electron beam irradiation, Adv. Sci. 10 (2023) 2205237, https://doi.org/10.1002/advs.202205237.
[137] R.F. Egerton, P. Li, M. Malac, Radiation damage in the TEM and SEM, Micron. 35 (2004) 399–409, https://doi.org/10.1016/j.micron.2004.02.003.
[138] H. Bei, E.P. George, Microstructures and mechanical properties of a directionally solidified NiAl–Mo eutectic alloy, Acta Mater. 53 (2005) 69–77, https://doi.org/10.1016/j.actamat.2004.09.003.
[139] H. Bei, Y.F. Gao, S. Shim, E.P. George, G.M. Pharr, Strength differences arising from homogeneous versus heterogeneous dislocation nucleation, Phys. Rev. B 77 (2008) 060103, https://doi.org/10.1103/PhysRevB.77.060103.
[140] F. Mompiou, M. Legros, A. Sedlmayr, D.S. Gianola, D. Caillard, O. Kraft, Source-based strengthening of sub-micrometer Al fibers, Acta Mater. 60 (2012) 977–983, https://doi.org/10.1016/j.actamat.2011.11.005.
[141] F. Mompiou, M. Legros, C. Ensslen, O. Kraft, In situ TEM study of twin boundary migration in sub-micron Be fibers, Acta Mater. 96 (2015) 57–65, https://doi.org/10.1016/j.actamat.2015.06.016.
[142] M. Chen, L. Pethö, A.S. Sologubenko, H. Ma, J. Michler, R. Spolenak, J. M. Wheeler, Achieving micron-scale plasticity and theoretical strength in Silicon, Nat. Commun. 11 (2020), https://doi.org/10.1038/s41467-020-16384-5 undefined-undefined.
[143] M. Chen, J. Wehrs, A.S. Sologubenko, J. Rabier, J. Michler, J.M. Wheeler, Size-dependent plasticity and activation parameters of lithographically-produced silicon micropillars, Mater. Des. 189 (2020) 108506, https://doi.org/10.1016/j.matdes.2020.108506.
[144] B. Moser, K. Wasmer, L. Barbieri, J. Michler, Strength and fracture of Si micropillars: a new scanning electron microscopy-based micro-compression test, J. Mater. Res. 22 (2007) 1004–1011, https://doi.org/10.1557/jmr.2007.0140.
[145] M. Chen, J. Wehrs, J. Michler, J.M. Wheeler, High-temperature In situ deformation of GaAs Micro-pillars: lithography versus FIB machining, JOM 68 (2016) 2761–2767, https://doi.org/10.1007/s11837-016-2106-8.
[146] C.A. Neugebauer, Tensile properties of thin, evaporated gold films, J. Appl. Phys. 31 (1960) 1096–1101, https://doi.org/10.1063/1.1735751.
[147] T.P. Weihs, S. Hong, J.C. Bravman, W.D. Nix, Mechanical deflection of cantilever microbeams: a new technique for testing the mechanical properties of thin films, J. Mater. Res. 3 (1988) 931–942, https://doi.org/10.1557/JMR.1988.0931.
[148] J.A. Ruud, D. Josell, F. Spaepen, A.L. Greer, A new method for tensile testing of thin films, J. Mater. Res. 8 (1993) 112–117, https://doi.org/10.1557/JMR.1993.0112.
[149] D.T. Read, J.W. Dally, A new method for measuring the strength and ductility of thin films, J. Mater. Res. 8 (1993) 1542–1549, https://doi.org/10.1557/JMR.1993.1542.
[150] R.D. Emery, G.L. Povirk, Tensile behavior of free-standing gold films. Part I. Coarse-grained films, Acta Mater. 51 (2003) 2067–2078, https://doi.org/10.1016/S1359-6454(03)00006-5.
[151] R.D. Emery, G.L. Povirk, Tensile behavior of free-standing gold films. Part II. Fine-grained films, Acta Mater. 51 (2003) 2079–2087, https://doi.org/10.1016/S1359-6454(03)00007-7.
[152] P.A. Gruber, C. Solenthaler, E. Arzt, R. Spolenak, Strong single-crystalline Au films tested by a new synchrotron technique, Acta Mater. 56 (2008) 1876–1889, https://doi.org/10.1016/j.actamat.2007.12.043.

[153] J. Böhm, P. Gruber, R. Spolenak, A. Stierle, A. Wanner, E. Arzt, Tensile testing of ultrathin polycrystalline films: a synchrotron-based technique, Rev. Sci. Instrument. 75 (2004) 1110–1119, https://doi.org/10.1063/1.1669124.
[154] W.N. Sharpe, J. Bagdahn, K. Jackson, G. Coles, Tensile testing of MEMS materials—recent progress, J. Mater. Sci. 38 (2003) 4075–4079, https://doi.org/10.1023/A:1026313102468.
[155] M.A. Haque, M.T.A. Saif, A review of MEMS-based microscale and nanoscale tensile and bending testing, Exp. Mech. 43 (2003) 248–255, https://doi.org/10.1007/BF02410523.
[156] W.N. Sharpe, K.T. Turner, R.L. Edwards, Tensile testing of polysilicon, Exp. Mech. 39 (1999) 162–170, https://doi.org/10.1007/BF02323548.
[157] M.A. Haque, M.T.A Saif, Mechanical behavior of 30–50 nm thick aluminum films under uniaxial tension, Scr. Mater. 47 (2002) 863–867, https://doi.org/10.1016/S1359-6462(02)00306-8.
[158] H.D. Espinosa, B.C. Prorok, M. Fischer, A novel experimental technique for testing thin films and MEMS materials, (2001).
[159] H.D. Espinosa, B.C. Prorok, B. Peng, Plasticity size effects in free-standing submicron polycrystalline FCC films subjected to pure tension, J. Mech. Phys. Solids 52 (2004) 667–689. https://doi.org/10.1016/j.jmps.2003.07.001.</bib.
[160] E.W. Backer, W. Ehrfeld, D. Münchmeyer, H. Betz, A. Heuberger, S. Pongratz, W. Glashauser, H.J. Michel, R.v. Siemens, Production of separation-nozzle systems for uranium enrichment by a combination of X-ray lithography and galvanoplastics, Naturwissenschaften. 69 (1982) 520–523. https://doi.org/10.1007/BF00463495.</bib.
[161] C. Beuret, G.-A. Racine, J. Gobet, R. Luthier, N.F. de Rooij, Microfabrication of 3D multidirectional inclined structures by UV lithography and electroplating, in: Proceedings IEEE Micro Electro Mechanical Systems An Investigation of Micro Structures, Sensors, Actuators, Machines and Robotic Systems, IEEE, Oiso, Japan, 1994, pp. 81–85. https://doi.org/10.1109/MEMSYS.1994.555602.</bib.
[162] H. Lorenz, M. Despont, P. Vettiger, P. Renaud, Fabrication of photoplastic high-aspect ratio microparts and micromolds using SU-8 UV resist, Microsyst. Technol. 4 (1998) 143–146, https://doi.org/10.1007/s005420050118.
[163] D. Zhang, J.-M. Breguet, R. Clavel, L. Philippe, I. Utke, J. Michler, In situ tensile testing of individual Co nanowires inside a scanning electron microscope, Nanotechnology. 20 (2009) 365706, https://doi.org/10.1088/0957-4484/20/36/365706.
[164] M.J. Burek, J.R. Greer, Fabrication and microstructure control of nanoscale mechanical testing specimens via electron beam lithography and electroplating, Nano Lett. 10 (2010) 69–76, https://doi.org/10.1021/nl902872w.
[165] A.T. Jennings, M.J. Burek, J.R. Greer, Microstructure versus Size: mechanical properties of electroplated single crystalline Cu nanopillars, Phys. Rev. Lett. 104 (2010) 135503, https://doi.org/10.1103/PhysRevLett.104.135503.
[166] G. Genolet, H. Lorenz, UV-LIGA: from development to commercialization, Micromachines. (Basel) 5 (2014) 486–495, https://doi.org/10.3390/mi5030486.
[167] A.G.N. Sofiah, M. Samykano, K. Kadirgama, R.V. Mohan, N.A.C. Lah, Metallic nanowires: mechanical properties – theory and experiment, Appl. Mater. Today 11 (2018) 320–337, https://doi.org/10.1016/j.apmt.2018.03.004.
[168] J.R. Greer, W.C. Oliver, W.D. Nix, Size dependence of mechanical properties of gold at the micron scale in the absence of strain gradients, Acta Mater. 53 (2005) 1821–1830, https://doi.org/10.1016/j.actamat.2004.12.031.
[169] D. Jang, X. Li, H. Gao, J.R. Greer, Deformation mechanisms in nanotwinned metal nanopillars, Nature Nanotech 7 (2012) 594–601, https://doi.org/10.1038/nnano.2012.116.
[170] X.Wendy Gu, Julia.R. Greer, Ultra-strong architected Cu meso-lattices, Extreme Mech. Lett. 2 (2015) 7–14, https://doi.org/10.1016/j.eml.2015.01.006.
[171] J.K. Gansel, M. Thiel, M.S. Rill, M. Decker, K. Bade, V. Saile, G. von Freymann, S. Linden, M. Wegener, Gold helix photonic metamaterial as broadband circular polarizer, Science (1979) 325 (2009) 1513–1515, https://doi.org/10.1126/science.1177031.
[172] P. Schürch, R. Ramachandramoorthy, L. Pethö, J. Michler, L. Philippe, Additive manufacturing by template-assisted 3D electrodeposition: nanocrystalline nickel microsprings and microspring arrays, Appl. Mater. Today 18 (2020) 100472, https://doi.org/10.1016/j.apmt.2019.100472.
[173] Z. Liu, N. Liu, J. Schroers, Nanofabrication through molding, Prog. Mater. Sci. 125 (2022) 100891, https://doi.org/10.1016/j.pmatsci.2021.100891.
[174] J. Xu, X. Wang, C. Wang, L. Yuan, W. Chen, J. Bao, Q. Su, Z. Xu, C. Wang, Z. Wang, D. Shan, B. Guo, A review on Micro/Nanoforming to fabricate 3D metallic structures, Adv. Mater. 33 (2021) 2000893, https://doi.org/10.1002/adma.202000893.
[175] S. Buzzi, F. Robin, V. Callegari, J.F. Löffler, Metal direct nanoimprinting for photonics, Microelectron. Eng. 85 (2008) 419–424, https://doi.org/10.1016/j.mee.2007.08.001.
[176] S. Buzzi, M. Galli, M. Agio, J.F. Löffler, Silver high-aspect-ratio micro- and nanoimprinting for optical applications, Appl. Phys. Lett. 94 (2009) 223115, https://doi.org/10.1063/1.3142426.
[177] L. Romano, J. Vila-Comamala, M. Kagias, K. Vogelsang, H. Schift, M. Stampanoni, K. Jefimovs, High aspect ratio metal microcasting by hot embossing for X-ray optics fabrication, Microelectron. Eng. 176 (2017) 6–10, https://doi.org/10.1016/j.mee.2016.12.032.
[178] D.J. Magagnosc, W. Chen, G. Kumar, J. Schroers, D.S. Gianola, Thermomechanical behavior of molded metallic glass nanowires, Sci. Rep. 6 (2016) 19530, https://doi.org/10.1038/srep19530.
[179] S. Buzzi, M. Dietiker, K. Kunze, R. Spolenak, J.F. Löffler, Deformation behavior of silver submicrometer-pillars prepared by nanoimprinting, Philos. Mag. 89 (2009) 869–884, https://doi.org/10.1080/14786430902791748.
[180] G. Baumeister, K. Mueller, R. Ruprecht, J. Hausselt, Production of metallic high aspect ratio microstructures by microcasting, Microsyst. Technol. 8 (2002) 105–108, https://doi.org/10.1007/s00542-001-0132-z.
[181] G. Baumeister, J. Hausselt, R. Ruprecht, Microcasting of parts made of metal alloys, Microsyst. Technol. 10 (2004) 261–264, https://doi.org/10.1007/s00542-003-0363-2.
[182] G. Baumeister, R. Ruprecht, J. Hausselt, Replication of LIGA structures using microcasting, Microsyst. Technol. 10 (2004) 484–488, https://doi.org/10.1007/s00542-004-0377-4.
[183] G. Baumeister, S. Rath, J. Hausselt, Microcasting of Al bronze and a gold base alloy improved by plaster-bonded investment, Microsyst. Technol. 12 (2006) 773–777, https://doi.org/10.1007/s00542-006-0105-3.
[184] G. Baumeister, D. Buqezi-Ahmeti, J. Glaser, H.-J. Ritzhaupt-Kleissl, New approaches in microcasting: permanent mold casting and composite casting, Microsyst. Technol. 17 (2011) 289–300, https://doi.org/10.1007/s00542-011-1237-7.
[185] L. Borasi, E. Casamenti, R. Charvet, C. Dénéréaz, S. Pollonghini, L. Deillon, T. Yang, F. Ebrahim, A. Mortensen, Y. Bellouard, 3D metal freeform micromanufacturing, J. Manuf. Process. 68 (2021) 867–876. https://doi.org/10.1016/j.jmapro.2021.06.002.</bib.
[186] H.W. Lee, M.A. Schmidt, R.F. Russell, N.Y. Joly, H.K. Tyagi, P. Uebel, P.S. J. Russell, Pressure-assisted melt-filling and optical characterization of Au nanowires in microstructured fibers, Opt. Express, OE 19 (2011) 12180–12189. https://doi.org/10.1364/OE.19.012180.</bib.
[187] S. Verheyden, L. Deillon, A. Mortensen, Stress relaxation in the presence of sudden strain bursts: methodology and stress relaxation data of microcast aluminium microwires, Data Brief 21 (2018) 2134–2141. https://doi.org/10.1016/j.dib.2018.11.047.</bib.
[188] S. Verheyden, L. Pires Da Veiga, L. Deillon, A. Mortensen, The effect of size on the plastic deformation of annealed cast aluminium microwires, Scr. Mater. 161 (2019) 58–61. https://doi.org/10.1016/j.scriptamat.2018.10.009.</bib.
[189] S.G.A. Verheyden, L. Deillon, A. Mortensen, The thermally activated deformation behaviour of single-crystalline microcast aluminium wires, Acta Mater. 234 (2022) 118037. https://doi.org/10.1016/j.actamat.2022.118037.</bib.
[190] L. Deillon, S. Verheyden, D. Ferreira Sanchez, S. Van Petegem, H. Van Swygenhoven, A. Mortensen, Laue microdiffraction characterisation of as-cast and tensile deformed Al microwires, Philos. Mag. 99 (2019) 1866–1880, https://doi.org/10.1080/14786435.2019.1605220.
[191] N. Kleger, S. Fehlmann, S.S. Lee, C. Dénéréaz, M. Cihova, N. Paunović, Y. Bao, J.-C. Leroux, S.J. Ferguson, K. Masania, A.R. Studart, Light-based printing of leachable salt molds for facile shaping of complex structures, Adv. Mater. 34 (2022) 2203878, https://doi.org/10.1002/adma.202203878.
[192] E. Casamenti, G. Torun, L. Borasi, M. Lautenbacher, M. Bertrand, J. Faist, A. Mortensen, Y. Bellouard, Glass-in-glass infiltration for 3D micro-optical composite components, Opt. Express, OE 30 (2022) 13603–13615, https://doi.org/10.1364/OE.451026.
[193] L. Borasi, A. Mortensen, Intermittent tensile deformation of silver microcastings: influence of the strain rate, Scr. Mater. 239 (2024) 115820, https://doi.org/10.1016/j.scriptamat.2023.115820.
[194] L. Borasi, A. Mortensen, On the slip burst amplitude cutoff in dislocation-rich microcrystals, Acta Mater. 264 (2024) 119582, https://doi.org/10.1016/j.actamat.2023.119582.
[195] T.A. Parthasarathy, S.I. Rao, D.M. Dimiduk, M.D. Uchic, D.R. Trinkle, Contribution to size effect of yield strength from the stochastics of dislocation source lengths in finite samples, Scr. Mater. 56 (2007) 313–316, https://doi.org/10.1016/j.scriptamat.2006.09.016.
[196] F. Mushtaq, M. Guerrero, M.S. Sakar, M. Hoop, A.M. Lindo, J. Sort, X. Chen, B. J. Nelson, E. Pellicer, S. Pané, Magnetically driven Bi2O3/BiOCl-based hybrid microrobots for photocatalytic water remediation, J. Mater. Chem. A 3 (2015) 23670–23676, https://doi.org/10.1039/C5TA05825B.
[197] S.-J. Jeon, J.-H. Lee, E.L. Thomas, Polyol synthesis of silver nanocubes via moderate control of the reaction atmosphere, J. Colloid Interface Sci. 435 (2014) 105–111, https://doi.org/10.1016/j.jcis.2014.08.039.
[198] D.F. Rojas, O.K. Orhan, M. Ponga, Dynamic recrystallization of Silver nanocubes during high-velocity impacts, Acta Mater. 212 (2021) 116892, https://doi.org/10.1016/j.actamat.2021.116892.
[199] R. Thevamaran, O. Lawal, S. Yazdi, S.-J. Jeon, J.-H. Lee, E.L. Thomas, Dynamic creation and evolution of gradient nanostructure in single-crystal metallic microcubes, Science (1979) 354 (2016) 312–316, https://doi.org/10.1126/science.aag1768.
[200] R. Thevamaran, C. Griesbach, S. Yazdi, M. Ponga, H. Alimadadi, O. Lawal, S.-J. Jeon, E.L. Thomas, Dynamic martensitic phase transformation in single-crystal silver microcubes, Acta Mater. 182 (2020) 131–143, https://doi.org/10.1016/j.actamat.2019.10.006.
[201] J.M. Wheeler, C. Niederberger, C. Tessarek, S. Christiansen, J. Michler, Extraction of plasticity parameters of GaN with high temperature, in situ micro-compression, Int. J. Plast. 40 (2013) 140–151, https://doi.org/10.1016/j.ijplas.2012.08.001.
[202] Y. Sun, Y. Xia, Shape-controlled synthesis of gold and silver nanoparticles, Science (1979) 298 (2002) 2176–2179, https://doi.org/10.1126/science.1077229.
[203] G. Žagar, V. Pejchal, M. Kissling, A. Mortensen, On the diametric compression strength test of brittle spherical particles, Eur. J. Mech. - A/Solids 72 (2018) 148–154, https://doi.org/10.1016/j.euromechsol.2018.04.016.
[204] V. Pejchal, M. Fornabaio, G. Žagar, G. Riesen, R.G. Martin, J. Medřický, T. Chráska, A. Mortensen, Meridian crack test strength of plasma-sprayed amorphous and nanocrystalline ceramic microparticles, Acta Mater. 145 (2018) 278–289, https://doi.org/10.1016/j.actamat.2017.12.031.

[205] S.S. Brenner, Tensile strength of whiskers, J. Appl. Phys. 27 (1956) 1484–1491, https://doi.org/10.1063/1.1722294.
[206] S.S. Brenner, Growth and properties of "Whiskers, Science (1979) 128 (1958) 569–575, https://doi.org/10.1126/science.128.3324.569.
[207] G. Richter, K. Hillerich, D.S. Gianola, R. Mönig, O. Kraft, C.A. Volkert, Ultrahigh strength single crystalline nanowhiskers grown by physical vapor deposition, Nano Lett. 9 (2009) 3048–3052, https://doi.org/10.1021/nl9015107.
[208] Y. Zhu, Mechanics of crystalline nanowires: an experimental perspective, Appl. Mech. Rev. 69 (2017), https://doi.org/10.1115/1.4035511.
[209] L.M. Vogl, P. Schweizer, G. Richter, E. Spiecker, Effect of size and shape on the elastic modulus of metal nanowires, MRS. Adv. 6 (2021) 665–673, https://doi.org/10.1557/s43580-021-00103-3.
[210] B. Khodashenas, H.R. Ghorbani, Synthesis of silver nanoparticles with different shapes, Arab. J. Chem. 12 (2019) 1823–1838, https://doi.org/10.1016/j.arabjc.2014.12.014.
[211] S. Maruo, O. Nakamura, S. Kawata, Three-dimensional microfabrication with two-photon-absorbed photopolymerization, Opt. Lett., OL 22 (1997) 132–134, https://doi.org/10.1364/OL.22.000132.
[212] S. Maruo, K. Ikuta, Three-dimensional microfabrication by use of single-photon-absorbed polymerization, Appl. Phys. Lett. 76 (2000) 2656–2658, https://doi.org/10.1063/1.126742.
[213] S. Kawata, H.-B. Sun, T. Tanaka, K. Takada, Finer features for functional microdevices, Nature 412 (2001) 697–698, https://doi.org/10.1038/35089130.
[214] X. Zhou, Y. Hou, J. Lin, A review on the processing accuracy of two-photon polymerization, AIP Adv. 5 (2015) 030701, https://doi.org/10.1063/1.4916886.
[215] D.W. Yee, M.D. Schulz, R.H. Grubbs, J.R. Greer, Functionalized 3D architected materials via Thiol-michael addition and two-photon lithography, Adv. Mater. 29 (2017) 1605293, https://doi.org/10.1002/adma.201605293.
[216] T.G. Pattison, S. Wang, R.D. Miller, G. Liu, G.G. Qiao, 3D nanoprinting via spatially controlled assembly and polymerization, Nat. Commun. 13 (2022) 1941, https://doi.org/10.1038/s41467-022-29432-z.
[217] L.R. Meza, A.J. Zelhofer, N. Clarke, A.J. Mateos, D.M. Kochmann, J.R. Greer, Resilient 3D hierarchical architected metamaterials, Proc. Natl. Acad. Sci. 112 (2015) 11502–11507, https://doi.org/10.1073/pnas.1509120112.
[218] R.D. Farahani, M. Dubé, D. Therriault, Three-dimensional printing of multifunctional nanocomposites: manufacturing techniques and applications, Adv. Mater. 28 (2016) 5794–5821, https://doi.org/10.1002/adma.201506215.
[219] B.G. Compton, J.A. Lewis, 3D-printing of lightweight cellular composites, Adv. Mater. 26 (2014) 5930–5935, https://doi.org/10.1002/adma.201401804.
[220] J. Bauer, C. Crook, T. Baldacchini, A sinterless, low-temperature route to 3D print nanoscale optical-grade glass, Science (1979) 380 (2023) 960–966, https://doi.org/10.1126/science.abq3037.
[221] P.-H. Huang, M. Laakso, P. Edinger, O. Hartwig, G.S. Duesberg, L.-L. Lai, J. Mayer, J. Nyman, C. Errando-Herranz, G. Stemme, K.B. Gylfason, F. Niklaus, Three-dimensional printing of silica glass with sub-micrometer resolution, Nat. Commun. 14 (2023) 3305, https://doi.org/10.1038/s41467-023-38996-3.
[222] A. Vyatskikh, R.C. Ng, B. Edwards, R.M. Briggs, J.R. Greer, Additive manufacturing of high-refractive-index, nanoarchitected titanium dioxide for 3D dielectric photonic crystals, Nano Lett. 20 (2020) 3513–3520, https://doi.org/10.1021/acs.nanolett.0c00454.
[223] Z. Chen, Z. Li, J. Li, C. Liu, C. Lao, Y. Fu, C. Liu, Y. Li, P. Wang, Y. He, 3D printing of ceramics: a review, J. Eur. Ceram. Soc. 39 (2019) 661–687, https://doi.org/10.1016/j.jeurceramsoc.2018.11.013.
[224] D.W. Yee, M.A. Citrin, Z.W. Taylor, M.A. Saccone, V.L. Tovmasyan, J.R. Greer, Hydrogel-based additive manufacturing of lithium cobalt oxide, Adv. Mater. Technol. 6 (2021) 2000791, https://doi.org/10.1002/admt.202000791.
[225] D.W. Yee, M.L. Lifson, B.W. Edwards, J.R. Greer, Additive manufacturing of 3D-architected multifunctional metal oxides, Adv. Mater. 31 (2019) 1901345, https://doi.org/10.1002/adma.201901345.
[226] G. Ercolano, T. Zambelli, C. van Nisselroy, D. Momotenko, J. Vörös, T. Merle, W. W. Koelmans, Multiscale additive manufacturing of metal microstructures, Adv. Eng. Mater. 22 (2020) 1900961, https://doi.org/10.1002/adem.201900961.
[227] B.Y. Ahn, E.B. Duoss, M.J. Motala, X. Guo, S.-I. Park, Y. Xiong, J. Yoon, R. G. Nuzzo, J.A. Rogers, J.A. Lewis, Omnidirectional printing of flexible, stretchable, and spanning silver microelectrodes, Science (1979) 323 (2009) 1590–1593, https://doi.org/10.1126/science.1168375.
[228] M.S. Onses, E. Sutanto, P.M. Ferreira, A.G. Alleyne, J.A. Rogers, Mechanisms, capabilities, and applications of high-resolution electrohydrodynamic jet printing, Small. 11 (2015) 4237–4266, https://doi.org/10.1002/smll.201500593.
[229] B. Zhang, J. He, X. Li, F. Xu, D. Li, Micro/nanoscale electrohydrodynamic printing: from 2D to 3D, Nanoscale 8 (2016) 15376–15388, https://doi.org/10.1039/C6NR04106J.
[230] P. Galliker, J. Schneider, H. Eghlidi, S. Kress, V. Sandoghdar, D. Poulikakos, Direct printing of nanostructures by electrostatic autofocussing of ink nanodroplets, Nat. Commun. 3 (2012) 890, https://doi.org/10.1038/ncomms1891.
[231] P. Galliker, J. Schneider, D. Poulikakos, Dielectrophoretic bending of directly printed free-standing ultra-soft nanowires, Appl. Phys. Lett. 104 (2014) 073105, https://doi.org/10.1063/1.4866002.
[232] J. Schneider, P. Rohner, D. Thureja, M. Schmid, P. Galliker, D. Poulikakos, Electrohydrodynamic NanoDrip printing of high aspect ratio metal grid transparent electrodes, Adv. Funct. Mater. 26 (2016) 833–840, https://doi.org/10.1002/adfm.201503705.
[233] S.K. Seol, D. Kim, S. Lee, J.H. Kim, W.S. Chang, J.T. Kim, Electrodeposition-based 3D printing of metallic microarchitectures with controlled internal structures, Small. 11 (2015) 3896–3902, https://doi.org/10.1002/smll.201500177.
[234] L. Hirt, S. Ihle, Z. Pan, L. Dorwling-Carter, A. Reiser, J.M. Wheeler, R. Spolenak, J. Vörös, T. Zambelli, Template-Free 3D microprinting of metals using a force-controlled Nanopipette for Layer-by-layer electrodeposition, Adv. Mater. 28 (2016) 2311–2315, https://doi.org/10.1002/adma.201504967.
[235] M.A. Saccone, R.A. Gallivan, K. Narita, D.W. Yee, J.R. Greer, Additive manufacturing of micro-architected metals via hydrogel infusion, Nature 612 (2022) 685–690, https://doi.org/10.1038/s41586-022-05433-2.
[236] A. Reiser, M. Lindén, P. Rohner, A. Marchand, H. Galinski, A.S. Sologubenko, J. M. Wheeler, R. Zenobi, D. Poulikakos, R. Spolenak, Multi-metal electrohydrodynamic redox 3D printing at the submicron scale, Nat. Commun. 10 (2019) 1853, https://doi.org/10.1038/s41467-019-09827-1.
[237] T. Tanaka, A. Ishikawa, S. Kawata, Two-photon-induced reduction of metal ions for fabricating three-dimensional electrically conductive metallic microstructure, Appl. Phys. Lett. 88 (2006) 081107, https://doi.org/10.1063/1.2177636.
[238] S. Daryadel, A. Behroozfar, M. Minary-Jolandan, A microscale additive manufacturing approach for in situ nanomechanics, Mater. Sci. Eng.: A 767 (2019) 138441, https://doi.org/10.1016/j.msea.2019.138441.
[239] J. Wang, R.C.Y. Auyeung, H. Kim, N.A. Charipar, A. Piqué, Three-dimensional printing of interconnects by laser direct-write of silver nanopastes, Adv. Mater. 22 (2010) 4462–4466, https://doi.org/10.1002/adma.201001729.
[240] L. Hirt, A. Reiser, R. Spolenak, T. Zambelli, Additive manufacturing of metal structures at the micrometer scale, Adv. Mater. 29 (2017) 1604211, https://doi.org/10.1002/adma.201604211.
[241] A. Reiser, L. Koch, K.A. Dunn, T. Matsuura, F. Iwata, O. Fogel, Z. Kotler, N. Zhou, K. Charipar, A. Piqué, P. Rohner, D. Poulikakos, S. Lee, S.K. Seol, I. Utke, C. Nisselroy, T. Zambelli, J.M. Wheeler, R. Spolenak, Metals by micro-scale additive manufacturing: comparison of microstructure and mechanical properties, Adv. Funct. Mater. 30 (2020) 1910491, https://doi.org/10.1002/adfm.201910491.
[242] R. Ramachandramoorthy, S. Kalácska, G. Poras, J. Schwiedrzik, T.E.J. Edwards, X. Maeder, T. Merle, G. Ercolano, W.W. Koelmans, J. Michler, Anomalous high strain rate compressive behavior of additively manufactured copper micropillars, Appl. Mater. Today 27 (2022) 101415, https://doi.org/10.1016/j.apmt.2022.101415.
[243] G. Žagar, V. Pejchal, M.G. Mueller, A. Rossoll, M. Cantoni, A. Mortensen, The local strength of microscopic alumina reinforcements, Acta Mater. 100 (2015) 215–223, https://doi.org/10.1016/j.actamat.2015.08.026.
[244] M.G. Mueller, G. Žagar, A. Mortensen, In-situ strength of individual silicon particles within an aluminium casting alloy, Acta Mater. 143 (2018) 67–76, https://doi.org/10.1016/j.actamat.2017.09.058.
[245] V. Pejchal, M. Fornabaio, G. Žagar, A. Mortensen, The local strength of individual alumina particles, J. Mech. Phys. Solids 109 (2017) 34–49, https://doi.org/10.1016/j.jmps.2017.08.005.
[246] A. Slagter, J. Everaerts, L. Deillon, A. Mortensen, Strong silicon oxide inclusions in iron, Acta Mater. 242 (2023) 118437, https://doi.org/10.1016/j.actamat.2022.118437.
[247] M.G. Mueller, M. Fornabaio, G. Žagar, A. Mortensen, Microscopic strength of silicon particles in an aluminium–silicon alloy, Acta Mater. 105 (2016) 165–175, https://doi.org/10.1016/j.actamat.2015.12.006.
[248] D. Hernández-Escobar, A. Slagter, S. Perosanz Amarillo, A. Mortensen, Room-temperature strength of the interfacial bond between silica inclusions and iron, Acta Mater. 263 (2024) 119502, https://doi.org/10.1016/j.actamat.2023.119502.
[249] K. Matoy, T. Detzel, M. Müller, C. Motz, G. Dehm, Interface fracture properties of thin films studied by using the micro-cantilever deflection technique, Surf. Coat. Technol. 204 (2009) 878–881, https://doi.org/10.1016/j.surfcoat.2009.09.013.
[250] H. Kahn, N. Tayebi, R. Ballarini, R.L. Mullen, A.H. Heuer, Fracture toughness of polysilicon MEMS devices, Sensor. Actuator. A: Phys. 82 (2000) 274.
[251] M. Sebastiani, K.E. Johanns, E.G. Herbert, F. Carassiti, G.M. Pharr, A novel pillar indentation splitting test for measuring fracture toughness of thin ceramic coatings, Philos. Mag. 95 (2015) 1928–1944, https://doi.org/10.1080/14786435.2014.913110.
[252] C.M. Lauener, L. Petho, M. Chen, Y. Xiao, J. Michler, J.M. Wheeler, Fracture of Silicon: influence of rate, positioning accuracy, FIB machining, and elevated temperatures on toughness measured by pillar indentation splitting, Mater. Des. 142 (2018) 340–349, https://doi.org/10.1016/j.matdes.2018.01.015.
[253] S. Liu, J.M. Wheeler, P.R. Howie, X.T. Zeng, J. Michler, W.J. Clegg, Measuring the fracture resistance of hard coatings, Appl. Phys. Lett. 102 (2013) 171907, https://doi.org/10.1063/1.4803928.
[254] G. Sernicola, T. Giovannini, P. Patel, J.R. Kermode, D.S. Balint, T.B. Britton, F. Giuliani, situ stable crack growth at the micron scale, Nat. Commun. 8 (2017) 108, https://doi.org/10.1038/s41467-017-00139-w.
[255] F.W. DelRio, S.J. Grutzik, W.M. Mook, S.M. Dickens, P.G. Kotula, E.D. Hintsala, D. D. Stauffer, B.L. Boyce, Eliciting stable nanoscale fracture in single-crystal silicon, Mater. Res. Lett. 10 (2022) 728–735, https://doi.org/10.1080/21663831.2022.2088251.
[256] B.N. Jaya, V. Jayaram, Crack stability in edge-notched clamped beam specimens: modeling and experiments, Int. J. Fract. 188 (2014) 213–228, https://doi.org/10.1007/s10704-014-9956-2.
[257] J.L. Mead, M. Lu, H. Huang, Inducing stable interfacial delamination in a multilayer system by four-point bending of microbridges, Surf. Coat. Technol. 320 (2017) 478–482, https://doi.org/10.1016/j.surfcoat.2016.11.069.
[258] Y. Hu, J.-H. Huang, J.-M. Zuo, In situ characterization of fracture toughness and dynamics of nanocrystalline titanium nitride films, J. Mater. Res. 31 (2016) 370–379, https://doi.org/10.1557/jmr.2016.4.

[259] N. Jaya B, V. Jayaram, S.K. Biswas, A new method for fracture toughness determination of graded (Pt,Ni)Al bond coats by microbeam bend tests, Philos. Mag. 92 (2012) 3326–3345, https://doi.org/10.1080/14786435.2012.669068.
[260] M.G. Mueller, V. Pejchal, G. Žagar, A. Singh, M. Cantoni, A. Mortensen, Fracture toughness testing of nanocrystalline alumina and fused quartz using chevron-notched microbeams, Acta Mater. 86 (2015) 385–395, https://doi.org/10.1016/j.actamat.2014.12.016.
[261] G. Žagar, V. Pejchal, M.G. Mueller, L. Michelet, A. Mortensen, Fracture toughness measurement in fused quartz using triangular chevron-notched micro-cantilevers, Scr. Mater. 112 (2016) 132–135, https://doi.org/10.1016/j.scriptamat.2015.09.032.
[262] E. Okotete, S. Brinckmann, S. Lee, C. Kirchlechner, How to avoid FIB-milling artefacts in micro fracture? A new geometry for interface fracture, Mater. Des. 232 (2023) 112134, https://doi.org/10.1016/j.matdes.2023.112134.
[263] W.C. Oliver, G.M. Pharr, Measurement of hardness and elastic modulus by instrumented indentation: advances in understanding and refinements to methodology, J. Mater. Res. 19 (2004) 3–20, https://doi.org/10.1557/jmr.2004.19.1.3.
[264] S.J. Bull, Nanoindentation of coatings, J. Phys. D: Appl. Phys. 38 (2005) R393, https://doi.org/10.1088/0022-3727/38/24/R01.
[265] A.C. Fischer-Cripps, Critical review of analysis and interpretation of nanoindentation test data, Surf. Coat. Technol. 200 (2006) 4153–4165, https://doi.org/10.1016/j.surfcoat.2005.03.018.
[266] C.A. Schuh, Nanoindentation studies of materials, Mater. Today 9 (2006) 32–40, https://doi.org/10.1016/S1369-7021(06)71495-X.
[267] J.M. Wheeler, D.E.J. Armstrong, W. Heinz, R. Schwaiger, High temperature nanoindentation: the state of the art and future challenges, Curr. Opin. Solid State Mater. Sci. 19 (2015) 354–366, https://doi.org/10.1016/j.cossms.2015.02.002.
[268] Yu.I. Golovin, Nanoindentation and mechanical properties of materials at Submicro- and Nanoscale levels: recent results and achievements, Phys. Solid State 63 (2021) 1–41, https://doi.org/10.1134/S1063783421010108.
[269] P. Sudharshan Phani, B.L. Hackett, C.C. Walker, W.C. Oliver, G.M. Pharr, High strain rate nanoindentation testing: recent advancements, challenges and opportunities, Curr. Opin. Solid State Mater. Sci. (2023) 101054, https://doi.org/10.1016/j.cossms.2022.101054.
[270] Y. Zhang, B.L. Hackett, J. Dong, K.Y. Xie, G.M. Pharr, Evolution of dislocation substructures in metals via high-strain-rate nanoindentation, Proc. Natl. Acad. Sci. 120 (2023) e2310500120, https://doi.org/10.1073/pnas.2310500120.
[271] G. Tiphéne, P. Baral, S. Comby-Dassonneville, G. Guillonneau, G. Kermouche, J.-M. Bergheau, W. Oliver, J.-L. Loubet, High-temperature scanning indentation: a new method to investigate in situ metallurgical evolution along temperature ramps, J. Mater. Res. 36 (2021) 2383–2396, https://doi.org/10.1557/s43578-021-00107-7.
[272] S. Comby-Dassonneville, G. Tiphéne, A. Borroto, G. Guillonneau, L. Roiban, G. Kermouche, J.-F. Pierson, J.-L. Loubet, P. Steyer, Real-time high-temperature scanning indentation: probing physical changes in thin-film metallic glasses, Appl. Mater. Today 24 (2021) 101126, https://doi.org/10.1016/j.apmt.2021.101126.
[273] A. Slagter, J. Everaerts, A. Mortensen, Nanoindentation of embedded particles, J. Mater. Res. 38 (2023) 1694–1705, https://doi.org/10.1557/s43578-023-00920-2.
[274] J.M. Wheeler, B. Gan, R. Spolenak, Combinatorial investigation of the Ni–Ta system via correlated high-speed nanoindentation and EDX mapping, Small. Methods 6 (2022) 2101084, https://doi.org/10.1002/smtd.202101084.